Clarification of Physiological Functions of Spindle Assembly Checkpoint Factor BubR1

A Dissertation Submitted to
the Graduate School of Life and Environmental Sciences,
the University of Tsukuba
in Partial Fulfillment of the Requirements
for the Degree of Doctor of Philosophy in Biological Science
(Doctoral Program in Biological Sciences)

Ayae YOSHIDA

Table of Contents

Abstract.....1

Abbreviations.....3

General Introduction.....5

Chapter 1

BubR1 insufficiency impairs liver regeneration in aged mice after hepatectomy through intercalated disc abnormality

Introduction.....10

Materials and Methods.....12

Results.....17

Discussion.....31

Chapter 2

Contribution of BubR1 to oxidative stress-induced aneuploidy in p53 deficient cells

Introduction.....37

Materials and Methods.....39

Results.....44

Discussion.....55

General Discussion.....59

Acknowledgements.....63

References.....64

Abstract

Budding uninhibited by benzimidazole-related 1 (BubR1) is a major factor of the spindle assembly checkpoint (SAC), which monitors the accurate separation of sister chromosomes. When SAC function is impaired, unequal chromosomal distribution occurs, resulting in aneuploidy. Loss-of-function mutations in the *Bub1b* gene, which encodes BubR1, cause premature chromatid separation syndrome, a congenital disease, due to impaired SAC function. In addition, BubR1 has SAC-independent functions, playing roles in cellular processes such as cilia formation and aging, and each of its functions appear to be related to human disease. Therefore, I hypothesized that elucidating further physiological functions of BubR1 might aid in the discovery of new disease mechanisms in humans.

In the first study, I investigated the relationship between BubR1 and impaired liver regeneration due to aging. Delayed liver regeneration after partial hepatectomy (PHx) is frequently observed in aged patients, and leads to acute liver injury. Low expression of BubR1 is also reportedly involved in aging; however, its effects on liver regeneration have not been investigated. Thus, I investigated the effects of BubR1 insufficiency on liver regeneration in mice. Low-BubR1-expressing mutant (*BubR1*$^{L/L}$) mice displayed delayed recovery of the liver weight-to-body weight ratio and increased liver deviation enzyme levels after PHx. Microscopic observation of *BubR1*$^{L/L}$ mouse livers demonstrated an increased number of necrotic hepatocytes and intercalated disc anomalies, resulting in widened inter-hepatocyte and perisinusoidal spaces, smaller hepatocytes, and early-stage microvilli atrophy. Up-regulation of desmocollin-1 (DSC1) was observed in wild type, but not in *BubR1*$^{L/L}$, mice after PHx. In addition, BubR1 knockdown caused the down-regulation of DSC1 in a human keratinocyte cell line. The data suggest that BubR1 insufficiency resulted in impaired liver regeneration through weakened microstructural adaptation against PHx, enhanced transient liver failure, and delayed hepatocyte proliferation.

In the second study, I investigated the contribution of BubR1 to carcinogenesis and tumor malignancy. Although there are numerous reports that high BubR1 expression is a poor prognostic maker for various tumors and that aneuploidy is observed in these tumors, the relationship between

these clinical findings and high BubR1 expression remains unclear. Therefore, I explored why high BubR1 expression occurs and how it relates to carcinogenesis and tumor malignancy. First, I examined the involvement of p53 signal pathway, a crucial molecule in avoiding aneuploidy, in the control of BubR1 expression. $KBrO_3$, an oxidant, caused the activation of p53 signaling pathway and suppressed BubR1 expression in human diploid fibroblast MRC5 cells. This suppression was dependent on functional p53 and reactive oxygen species. In p53-depleted cells, $KBrO_3$ did not suppress BubR1 expression and caused increases in both binucleated cells and cells with > 4N DNA content. BubR1 downregulation suppressed $KBrO_3$-induced binucleation and cells with > 4N DNA content in p53 knockdown cells, suggesting that BubR1 contributes to enhanced polyploidization. In an analysis of 182 gastric cancer specimens, BubR1 expression was significantly higher p53 was positively stained, which indicates loss of p53 function (p= 0.0019). Moreover, p53 positivity and high BubR1 expression in tumors were significantly correlated with aneuploidy (p=0.0065). These observations suggest that p53 deficiency may lead to failure to downregulate BubR1, and p53 deficiency and BubR1 accumulation could contribute to gastric carcinogenesis associated with aneuploidy.

These studies reinforce the notion that BubR1 is associated with biologically important processes, both as part of the SAC and independently. Since abnormal expression of BubR1 results in various diseases, it is considered a useful target for drug development. In the future, it will be necessary to elucidate the factors affecting each function downstream of BubR1. Moreover, further clarification of the relationships between different BubR1 functions at the molecular level will lead to the elucidation of new disease mechanisms, and contribute to the development of effective treatments for BubR1-related diseases.

Abbreviations

BubR1: budding uninhibited by benzimidazole-related 1

SAC: spindle assembly checkpoint

APC/C: anaphase-promoting complex/cyclosome

CDC20: cell-division cycle protein 20

CDK1: cyclin-dependent kinase 1

MCC: mitotic checkpoint complex

Mad2: mitotic arrest deficient 2

Bub3: budding uninhibited by benzimidazoles 3 homolog

Mad3: mitotic arrest deficient 3

PCS: premature chromatid separation

MVA: mosaic variegated aneuploidy

PHx: partial hepatectomy

ID: intercalated disc

DSC1: desmocollin-1

ALT: alanine:2-oxoglutarate aminotransferase

AST: asparate:2-oxoglutarate aminotransferase

LDH: lactate dehydrogenase

T-BIL: total bilirubin

D-BIL: direct bilirubin

I-BIL: indirect bilirubin

TBA: total bile acid

ALP: alkaline phosphatase

IDs: intercalated disks

DICD: detachment induced cell death

mRNA: messenger ribonucleic acid

siRNA: small interfering RNA

PCR: polymerase chain reaction

HaCaT cells: human keratinocyte cell line

General Introduction

Cell division is necessary for the development and maintenance of life, and occurs through the replication and even distribution of cellular components to two daughter cells. For the survival and evolution of species, division must occur accurately, and thus each step is controlled by cell cycle control mechanisms. One of these control mechanisms, the spindle assembly checkpoint (SAC), monitors whether chromosomes are evenly distributed to daughter cells. During DNA replication, replicated sister chromatids are attached to each other by a protein complex called cohesin. Upon entering mitosis, the kinetochore, a protein complex located at the centromere of each chromatid, binds microtubules extending from opposite poles of the cell. With proper kinetochore-microtubule attachment, the multisubunit ubiquitin E3 ligase, anaphase-promoting complex/cyclosome (APC/C) associates with a specific coactivator called cell division cycle 20 (CDC20), and ubiquitinates and degrades two key proteins maintaining the cell in prometaphase: cyclin B and securin. Cyclin B is a regulatory subunit of the master mitotic kinase cyclin-dependent kinase 1 (CDK1) and securin is an inhibitor of separase, a cohesin protease. Proteolysis of these proteins leads to the separation of sister chromatids (Bolanos-Garcia et al. 2011). However, if a kinetochore is improperly attached to the microtubules, multiple SAC factors associate there, forming the mitotic checkpoint complex (MCC), which incorporates CDC20 and interferes with APC/C activation, delaying anaphase onset and giving the cell time to correct attachment errors. Once proper attachment is achieved, the MCC is dismantled and the APC/C is activated, allowing progression to anaphase. Defects in the SAC allow cells with improperly attached kinetochores to enter anaphase, generating aneuploid cells. BubR1 (budding uninhibited by benzimidazole-related 1) forms the MCC with mitotic arrest deficient-like 1 (Mad2), Bub3 and CDC20, and plays a key role in SAC function (Yu 2002).

BubR1 is a metazoan homologue of yeast (*Saccharomyces cerevisiae*) Mad3. The general domain architecture of BubR1 is shown in Fig 1. Human (*Homo sapiens*) BubR1 is 1050 residues long and can be divided into three regions on both structural and functional grounds: the N-terminal region (residues 1–426), containing most of the sequence conserved with yeast Mad3, the C-terminal region (residues 730–1050) containing the kinase domain, and a middle region (residues 427–729).

Figure 1. Schematic of the structure of BubR1 and Mad3.

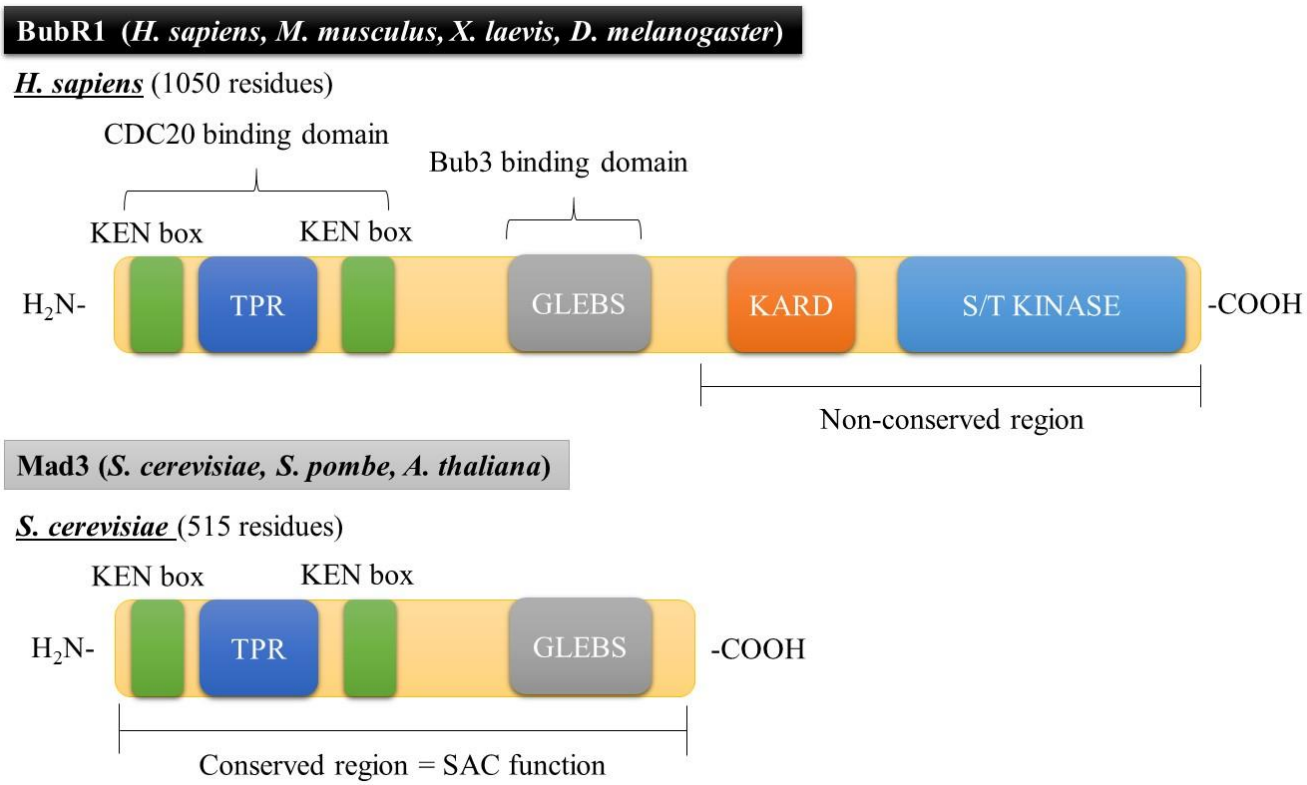

Two Lys-Glu-Asn (KEN) box motifs, three tetratricopeptide repeat (TPR) motifs, and one Gle2 (nucleoporin)-binding-sequence (GLEBS) motif are located in the conserved region and contribute to SAC function. The kinetochore attachment regulatory domain (KARD) and serine/threonine (S/T) kinase domain are in the non-conserved region of BubR1. The KARD may promote proper kinetochore-microtubule attachments. The function of S/T kinase domain is controversial. *H. sapiens*, *Homo sapiens*; *M. musculus*, *Mus musculus*; *X. laevis*, *Xenopus laevis*; *D. melanogaster*, *Drosophila melanogaster*; *S. cerevisiae*, *Saccharomyces cerevisiae*; *S. pombe*, *Schizosaccharomyces pombe*, and *A. thaliana*, *Arabidopsis thaliana*. The residue numbers in each domain of *H. sapiens* BubR1 and *S. cerevisiae* Mad3 are shown in parentheses below the domain abbreviations.

The N-terminal region is the most highly conserved across eukaryotes, and is involved in MCC formation and SAC function. The middle region is involved in promoting stable kinetochore and microtubule attachments (Karess et al. 2013). The function of serine/threonine (S/T) kinase domain is controversial.

Loss-of-function mutations in *Bub1b*, which encodes BubR1, cause premature chromatid separation (PCS) syndrome (Mendelian Inheritance in Man [MIM] 176430), a congenital disease also known as mosaic variegated aneuploidy (MVA) syndrome (MIM 257300) (Hanks et al. 2004, Matsuura et al. 2006). PCS/MVA syndrome can be caused by the suppression of *Bub1b* transcription by an intergenic mutation 44-kb upstream of the *Bub1b* gene (Ochiai et al. 2014). PCS/MVA syndrome is diagnosed by the presence of PCS in > 50% of metaphase cells and the presence of mosaic aneuploidy. Patients are more prone to develop childhood cancers such as Wilms tumor and rhabdomyosarcoma, which may be attributed to loss of SAC function. Obesity, polycystic kidneys, postcerebellar cysts, and hypoplasia of the cerebellar vermis are also common clinical findings, but the pathophysiological mechanisms of these features are unknown. In recent years, it has been postulated that these could be caused by SAC-independent BubR1 functions.

The primary cilium is a microtubule-based, nonmotile organelle that forms on the surface of quiescent mammalian cells (Nigg et al. 2009). It receives extracellular information and transmits signals required for cell proliferation, tissue development, and tissue homeostasis. Ciliary dysfunction results in human disorders known as ciliopathies (Baker et al. 2009) and affected patients show a series of clinical features including polycystic kidneys, polydactyly, obesity, and neuronal and other developmental abnormalities, similar to patients with PCS/MVA. Interestingly, impaired ciliogenesis was observed in skin fibroblasts from patients with PCS/MVA with mutations in *Bub1b* (Miyamoto et al. 2011), suggesting a link between ciliary dysfunction and loss of BubR1 function. Moreover, knockdown medaka fish (*Oryzias latipes*) displays ciliary dysfunction and typical phenotypes of ciliopathies (Miyamoto et al. 2011). These lines of evidence suggest that BubR1 plays an important, SAC-independent role in primary cilia formation.

BubR1 hypomorphic mice, with approximately 11% of the expression observed in wild type mice, show several early aging phenotypes, including short lifespan, cachectic dwarfism, lordokyphosis, sarcopenia, cataracts, craniofacial dysmorphisms, arterial stiffening, fat loss, reduced stress tolerance, and impaired wound healing (Baker et al. 2004). It was demonstrated that low BubR1expression in these mice induces $p16^{Ink4a}$ (a CDK1 inhibitor and marker of senescence) and promotes the development of aging-related phenotypes independently of SAC function (Baker et al. 2008, Baker et al. 2011). Interestingly, BubR1 mRNA and protein levels naturally decrease with aging in mice and humans (Baker et al. 2004, Guntani et al. 2011). These findings suggest a role for BubR1 in the natural aging process.

Clearly, BubR1 is a multifunctional protein, and both its SAC-dependent and -independent functions are suggested to be related to human disease. Therefore, I hypothesized that elucidating further physiological functions of BubR1 might aid in the discovery of new disease mechanisms in humans.

Since decreased BubR1 expression contributes to aging-related phenotypes, I have investigated the relationship between BubR1 and impaired liver regeneration due to aging (Chapter 1). In addition, although numerous reports suggest that high BubR1 expression could be a poor prognostic maker for various tumors (Grabsch et al. 2003, Burum-Auensen et al. 2007, Yamamoto et al. 2007), and that aneuploidy was observed in these tumors (Pinto et al. 2008, Ando et al. 2010), the relationships between these clinical findings and BubR1 expression remain unclear. Thus, I have also investigated the contribution of BubR1 to carcinogenesis and tumor malignancy (Chapter 2). Based on the results of these studies, I then discuss future directions for functional BubR1 research, and a strategy for drug development for BubR1-related diseases.

Chapter 1

BubR1 insufficiency impairs liver regeneration in aged mice after hepatectomy through intercalated disc abnormality

Introduction

It was previously demonstrated that decreased BubR1 expression induces cellular senescence through $p16^{INK4a}$ up-regulation, and that mutant mice with decreased BubR1 expression display various progeroid phenotypes, such as short lifespan, cachectic dwarfism, lordokyphosis, cataracts, loss of subcutaneous fat and impaired wound healing (Baker et al. 2004, Matsumoto et al. 2007, Baker et al. 2008, Baker et al. 2011). Therefore, BubR1 could play an important role in regulating aging. Kyuragi et al recently generated a new *BubR1* low-expression mouse, which is a useful model to investigate the role of BubR1 in response to various kinds of stress because they do not display any severe phenotypes during growth and development under normal circumstances (Kyuragi et al. 2015). Using this animal model, they have shown that reduced BubR1 expression inhibits intimal hyperplasia mediated by reduced vascular smooth muscle cell proliferation after carotid artery ligation.

Adult hepatocytes are normally quiescent cells in the G0 phase of the cell cycle and do not undergo cell division, whereas they proliferate to maintain liver homeostasis in response to several stimuli, such as surgical resections or liver injury (Fausto 1994, Michalopoulos et al. 1997). After partial hepatectomy (PHx), most of the quiescent hepatocytes (95% in young and 75% in old rats) rapidly enter the cell cycle (Michalopoulos 2007). In the mouse liver, peak DNA synthesis occurs at about 36–44 h after PHx, and DNA synthesis is synchronously initiated in hepatocytes (Matsuo et al. 2003, Taub 2004, Michalopoulos 2007). When DNA synthesis is impaired, hepatic regeneration is also impaired (Rudolph et al. 2000, Satyanarayana et al. 2003). Most of the increase in liver mass occurs within 3 days after PHx and the remnant liver regenerates to a size equivalent to the original volume within 5–7 days (Grisham 1962).

In animal models, hepatocytes are directly damaged and thereby induced to undergo necrosis or apoptosis to eliminate damaged cells after PHx (Guicciardi et al. 2013). Hepatocyte proliferation is initiated by several growth factors or cytokines during liver regeneration that occurs after massive hepatocyte necrosis or apoptosis (Fausto et al. 2006). The liver architecture during regeneration after PHx is significantly changed, and this change impacts liver function. Intra- and

inter-cellular junctions temporarily change during regeneration following PHx and reformation of the normal liver architecture occurs only after the original volume is restored. The mechanisms that regulate the reorganization of the liver architecture are not well understood (Taub 2004).

Liver regeneration is series of physio-pathological phenomena that allow recovery of damaged tissue and prevent liver failure (Haga et al. 2010). Impairment of liver regeneration is a critical problem for aged patients with liver diseases after surgical resection and PHx because their liver does not have the ability to regenerate physically and functionally. In the clinical setting, impairment of liver regeneration leads to liver dysfunction, which can worsen or affect the patient's general condition and their postoperative prognosis. The operative mortality rate for patients after major hepatectomy increased incrementally with age (Fortner et al. 1990). Aging impairs liver regeneration and there is a reduced rate of hepatocyte proliferation following resection (Schmucker et al. 2011). However, the mechanism of impaired regenerative capacity in the aged liver has not been fully elucidated.

A previous study suggests that BubR1 insufficiency causes early onset of aging-associated phenotypes (Baker et al. 2004), but the physiological relevance of BubR1 to liver regeneration and/or the effects of BubR1 on liver architecture remain unclear. The purpose of this study is to investigate the effects of BubR1 insufficiency on liver regeneration and its architecture using *BubR1* low-expression mice.

Materials and Methods

Experimental animals.

Animals were maintained under standard conditions and treated according to the Guidelines for the Care and Use of Laboratory Animals of Kyushu University. All experimental protocols were approved by the Kyushu University Institutional Animal Care and Use Committee. (Approval no. A24-220-0). Low-*BubR1*-expressing mutant (*BubR1*$^{L/L}$) and wild-type (WT) littermate control (*BubR1*$^{+/+}$) mice on a mixed genetic background of C57BL/6J/ and 129/SvJ were generated in the laboratory, as previously described. Five-week-old *BubR1*$^{L/L}$ and *BubR1*$^{+/+}$ male mice were used for experiments. Young (7-week-old) and aged (53-week-old) C57BL/6JJcl male mice were obtained from CLEA Japan Inc. (Tokyo, Japan), and kept in my facility for 2 weeks before use.

Partial hepatectomy model.

Seventy percent PHx was performed as previously described (Greene et al. 2003, Haga et al. 2010). Briefly, the bilateral median lobe and left lateral lobe were ligated and removed. After the wounds were sutured, animals were kept on a warming mat to avoid hypothermia. Mice were sacrificed to collect the remaining lobes and blood samples at each indicated time point before and after PHx. The liver weight-to-body weight ratio (LW/BW) was calculated to estimate liver mass recovery. Liver tissue samples were frozen or fixed with formalin and embedded in paraffin. Blood samples were collected from the postcava during anesthesia.

Biochemical analyses.

Asparate:2-oxoglutarate aminotransferase (AST), alanine:2-oxoglutarate aminotransferase (ALT), lactate dehydrogenase (LDH), total bilirubin (T-BIL), direct bilirubin (D-BIL), indirect bilirubin (I-BIL), total bile acid (TBA), and alkaline phosphatase (ALP) plasma levels were analyzed by Nagashima Life Sciences Laboratory (Shiga, Japan).

Cell culture.

A human keratinocyte cell line (HaCaT, Cell Lines Service, Eppelheim, Germany) was cultured in Dulbecco's Modified Eagle's Medium (DMEM, Thermo Fisher Scientific Inc., Waltham, MA, USA), supplemented with 10% heat-inactivated fetal bovine serum (FBS, Sigma-Aldrich Corp, St. Louis, MO, USA), 100 U/ml penicillin and 100 μg/ml streptomycin (Thermo Fisher Scientific Inc.) in plastic disposable tissue culture flasks for RNA extraction and coverslips for confocal laser scanning microscopy at 37°C in a 5% CO_2/95% air incubator.

BubR1 knockdown using siRNA.

Lipofectamine RNAiMAX transfection reagent (Life Technologies, Carlsbad, CA, USA) was used to transfect a siRNA targeting BubR1 (sc-37542; Santa Cruz Biotechnology, Dallas, TX, USA) or negative control (12935-112; Thermo Fisher Scientific Inc.) into HaCaT cells at a final concentration of 5 nmol/L in transfection reagent (dilution, 1:1000; vol/vol), according to the manufacturer's protocol. After siRNA transfection at 24, 48 and 72 h, siRNA-transfected HaCaT cells were collected. Total RNA was extracted and reverse-transcription was performed to obtain cDNA. BubR1 and desmocollin-1 (DSC1) mRNA expression was evaluated using quantitative real-time polymerase chain reaction (qRT-PCR). For confocal laser scanning microscopy, cells were fixed with ice-cold methanol after siRNA transfection at 48h.

mRNA quantification using qRT-PCR.

Total RNA was isolated using ISOGEN (Nippongene, Tokyo, Japan) and cDNAs were synthesized from RNAs using SuperScript III First-Strand Synthesis SuperMix (Thermo Fisher Scientific Inc.) according to the manufacturer's instructions. qRT-PCR amplification was performed using Applied Biosystems StepOnePlus Real-Time PCR System (Thermo Fisher Scientific Inc.). The primer/probe sets for mouse Ccnd1 (Mm00432359_m1), Ccne1 (Mm00432367_m1), Ccna2 (Mm00438064_m1), Ccnb2 (Mm01171453_m1), p21 (Mm04205640_g1), p16 (Mm00494449_m1) and desmocollin-1 (Mm00496525_m1) from the TaqMan gene expression assays (Thermo Fisher Scientific Inc.) and the primer/probe set for β-actin (Mm00607939_s1) as a mouse endogenous

control were purchased from Thermo Fisher Scientific Inc. The primer/probes sets for human desmocollin-1 (Hs00245189_m1) and BubR1 (Hs02758991_g1) from the TaqMan gene expression assays (Thermo Fisher Scientific Inc.) and the primer/probe set for glyceraldehyde-3-phosphate dehydrogenase (GAPDH, Hs02758991_g1) as a human endogenous control were purchased from Applied Biosystems (Haga et al. 2010). Mouse BubR1 expression was analyzed using QuantiFast SYBR Green PCR kit (QIAGEN, Tokyo, Japan) and normalized to GAPDH, as previously described (Kyuragi et al. 2015). The sequences of primers are as follows: mouse BubR1, 5′-CAG TCC CAG CAC AGA CAG TTC CA-3′ (forward) and 5′-GCT AGC GAG CTT CTC TGT GGT TCA-3′ (reverse); and GAPDH 5′-ATC TGG AAA GCT GTG GCG-3′ (forward) and 5′-CCA CGA CGG ACA CAT TG-3′ (reverse).

Tissue histopathological examination.

Hematoxylin-eosin (HE) staining and silver impregnation stain were performed on 10% formalin-fixed and 3-μm paraffin-embedded sections of liver tissue. For transmission electron microscopic observation, liver samples were fixed in glutaraldehyde. Immunostaining was performed to detect proliferating cell nuclear antigen (PCNA; M0879, Dako, Tokyo, Japan) and streptavidin–biotin–peroxidase staining was performed using Histofine SAB-PO (M) immunohistochemical staining kit (Nichirei Bioscience Inc., Tokyo, Japan) and counterstained with hematoxylin. At least 1000 hepatocytes were counted for the mitotic index and PCNA positivity in different sections for each group. The necrosis score was calculated by counting the number of necrotic lesions per low-power magnification (×40) in 8 fields per slide.

Formalin-fixed/paraffin-embedded tissue specimens were used for immunofluorescence staining. Deparaffinization was performed by soaking in xylene for 5 min (twice), 100% ethanol for 3 min, 95% ethanol for 3 min, 85% ethanol for 3 min, 75% ethanol for 3 min and washing with PBS for 5 min. The sections were pretreated by autoclaving (121°C) for 20 min in 0.01 mol/L citrate-buffered saline (pH 6.0) for antigen retrieval. Non-specific reactions were blocked with 10% goat serum (Histofine SAB-PO(R) kit, Nichirei Bioscience Inc.) for 10 min. The sections were incubated with

rabbit polyclonal antibodies against DSC1 (LS-C167539, 1:50; LifeSpan BioSciences, Seattle, WA, USA) at 4°C overnight, before washing with PBS. The sections were incubated with anti-rabbit immunofluorescence antibodies (Alexa Fluor 555, 1:200, Abcam) to detect DSC1 for 60 min and washed 3 times with PBS for 5 min each.

Confocal Laser Scanning Microscopy.

siRNA mediated HaCaT cells were rinsed in PBS at 37 °C, fixed in cold methanol for 3 min at −20 °C, blocked (PBS containing 2% BSA and 2% normal goat serum) for 30 min at room temperature, and incubated with the following antibodies at the indicated dilution: rat anti-DSC1 at 1:100 (MAB7367; R&D Systems, Inc., Minneapolis, MN USA), rabbit anti-BubR1 at 1:100 (612503; BD Biosciences, San Jose, CA). Cells were rinsed in PBS at 37 °C, fixed in 4% paraformaldehyde for 15 min at 37 °C, permeabilized (PBS containing 0.2% Triton X-100) for 5 min at room temperature, blocked (PBS containing 2% BSA and 2% normal goat serum) for 30 min at room temperature. Secondary antibodies conjugated to Alexa Fluor 488, 555 (Molecular Probes) were used at 1:2,000 dilution. After a wash in PBS containing 4,6-diamidino-2-phenylindole (DAPI) for 5 min, the coverslips were mounted in ProLong Gold (Thermo Fisher). Fluorescence image acquisition was performed using a Nikon A1R confocal imaging system controlled by the Nikon NIS Elements software (Nikon). The objective lens was an oil immersion Plan-Apo × 60 numerical aperture (NA) 1.40 lens (Nikon). Images were acquired as Z-stacks at 0.2-μm intervals and maximum-intensity projections were generated using the NIS Elements software (Nikon).

Western blot analysis.

Western blot analysis was performed as previously described (Liu et al. 2012). Livers were isolated and all surrounding material was removed. After preparing lysates, proteins were separated using SDS-PAGE and transferred to a nylon membrane. The blots were probed with primary antibody for DSC1 (LS-C 167539, 1:500, LifeSpan BioSciences). Equal loading was confirmed using β-actin

(#4970, 1:1000, Cell Signaling Technology Inc.). Results are representative of three independent animals of each genotype at each age.

Enzyme-linked immunosorbent assay for hepatocyte growth factor.

Frozen liver tissue was homogenized in lysis buffer (CelLytic MT Cell Lysis Reagent, Sigma Aldrich, St. Louis, MO, USA) containing protease inhibitor cocktail (Nacalai Tesque, Kyoto, Japan) and hepatic hepatocyte growth factor (HGF) levels were measured using the Mouse/Rat HGF Quantikine ELISA Kit (R&D Systems, Minneapolis, MN, US). HGF levels were normalized to total protein levels in the liver tissue, as measured using a Bio-Rad Protein Assay (Bio-Rad, Hercules, CA, USA).

Statistical analysis.

Data were presented as the mean±standard deviation (SD). The Student's *t*-test was performed using JMP pro (version 9.0.0, SAS Institute Inc., Cary, NC, USA). Additional professional statistical assistance was provided by Junji Kishimoto, Kyushu University. Differences were considered to be significant at $p<0.05$.

Results

BubR1 mRNA expression in liver regeneration after partial hepatectomy.

BubR1 mRNA expression levels in the liver are shown in Fig. 2A, B and C. In *BubR1*$^{L/L}$ mice, BubR1 mRNA expression was significantly lower (0.11±0.09, $p<0.01$) than that of *BubR1*$^{+/+}$ mice (1.00±0.67; Fig. 2A). BubR1 expression (0.62±0.26, $p<0.05$) was significantly decreased in aged mice compared with young mice (1.00±0.26; Fig. 2B). Fig. 2C revealed an alteration of BubR1 mRNA expression after PHx in *BubR1*$^{L/L}$ mice and *BubR1*$^{+/+}$ mice. In *BubR1*$^{+/+}$ mice, BubR1 mRNA expression was significantly increased after PHx and reached a maximum level 48 h after PHx (18.55±6.92). In *BubR1*$^{L/L}$ mice, the expression level was low, similar to that observed in untreated *BubR1*$^{L/L}$ mice. In addition, BubR1 expression was delayed in *BubR1*$^{L/L}$ mice.

The LW/BW was compared in *BubR1*$^{+/+}$ and *BubR1*$^{L/L}$ mice (Fig. 2D), and in young and aged mice (Fig. 2E). In all groups, LW/BW was significantly decreased 12 h after PHx. LW/BW was significantly lower in *BubR1*$^{L/L}$ mice (0.025±0.006, $p<0.05$) compared with *BubR1* $^{+/+}$ mice (0.034±0.006) 48 h after PHx (Fig. 2D), and significantly lower in aged mice (0.033±0.002, $p<0.05$) compared with young mice (0.037±0.001) 144 h after PHx (Fig. 2E). The delay in liver regeneration did not cause significant change in mortality between BubR1$^{+/+}$ and BubR1$^{L/L}$ mice at any time point after PHx.

Biochemical analysis during liver regeneration.

Tables 1 and 2 show serial changes in laboratory data of mice with PHx. Plasma AST, ALT and LDH levels were dramatically increased 12 h after PHx in *BubR1*$^{L/L}$ and *BubR1*$^{+/+}$ mice, and these values were significantly higher in *BubR1*$^{L/L}$ mice than in *BubR1*$^{+/+}$ mice 12–24h after PHx (Table 1). In addition, plasma T-BIL, D-BIL, I-BIL, TBA and ALP levels were significantly higher in *BubR1*$^{L/L}$ mice 24 h after PHx. These data indicate that, in *BubR1*$^{L/L}$ mice, impaired liver function continues for a longer period compared with *BubR1*$^{+/+}$ mice. The effect of aging on liver dysfunction after PHx was also examined, and levels of plasma AST, ALT and LDH 24–48 h after PHx were significantly greater in aged mice than those in young mice (Table 2).

BubR1 insufficiency caused an abnormal cell-cycle progression in hepatocyte after partial hepatectomy.

To investigate the underlying mechanisms of impaired liver regeneration in *BubR1*$^{L/L}$ mice, I examined alterations of proliferation markers after PHx (Fig. 3A, B). In *BubR1*$^{+/+}$ mice, the number of PCNA-positive hepatocytes (185.7±63.5 vs. 1.69±2.16, p<0.01) and those undergoing mitosis (16.9±10.7 vs. 2.59±5.80, p<0.05) significantly increased 48 h after PHx compared with those 12 h after PHx. Such increases of both values were not observed in *BubR1*$^{L/L}$ mice (PCNA, 54.3±56.7; mitosis, 2.0±2.9). Fig. 3C shows the representative liver sections at 12, 24, 48, 96, 144 hours after PHx stained for PCNA in *BubR1*$^{L/L}$ and *BubR1*$^{+/+}$ mice. The peak of hepatocyte proliferation is observed 48 h after PHx in normal mice (Lehmann et al. 2012). Slow progression of hepatocyte proliferation was evident in *BubR1*$^{L/L}$ mice 48 h after PHx and thereafter.

Based on reduced hepatocyte proliferation, I also investigated cyclin-D, cyclin-E, cyclin-A and cyclin-B mRNA expression levels (Fig. 3D). In *BubR1*$^{L/L}$ mice, cyclin-D (0.93±0.44, p<0.05), cyclin-A (0.23±0.07, p<0.01) and cyclin-B (0.10±0.05, p<0.01) mRNA expression levels were significantly lower compared with those of *BubR1*$^{+/+}$ mice (1.71±0.47, 0.87±0.27 and 0.32±0.13, respectively) 12 h after PHx. The expression patterns of cyclin-D in *BubR1*$^{+/+}$ and *BubR1*$^{L/L}$ mice were different: two peaks at 12 and 48 h after PHx were observed in *BubR1*$^{+/+}$ mice while a single but broader peak was observed in *BubR1*$^{L/L}$ mice. In *BubR1*$^{+/+}$ mice, cyclin-A and cyclin-B mRNA expression showed remarkable increases 48 h after PHx, and rapidly decreases 96 h after PHx. Cyclin-B mRNA expression was significantly attenuated in *BubR1*$^{L/L}$ mice (5.6±4.6, p<0.05) compared with *BubR1*$^{+/+}$ mice (21.3±12.5) 48 h after PHx. These low expression levels continued up to 144 h after PHx without a rapid decrease. Similar patterns were observed in the expression of cyclin-A. Cyclin-E mRNA expression was significantly higher in *BubR1*$^{L/L}$ mice (1.4±0.4, p<0.05) compared with *BubR1*$^{+/+}$ mice (0.8±0.4) 24 h after PHx.

I also examined the expression of a CDK inhibitor, p21 (Fig. 3E). In *BubR1*$^{L/L}$ mice, p21 mRNA expression (3.51±1.51, p<0.05) was significantly higher than that in *BubR1*$^{+/+}$ mice (1.74±0.76) 24 h after PHx. I also examined the mRNA expression of p16^{INK4a}, another CDK

inhibitor, because it is reported that down-regulation of BubR1 causes up-regulation of p16 ^{INK4a} expression and induces cellular senescence (Baker et al. 2008, Baker et al. 2011). In my study, however, p16 ^{INK4a} mRNA expression was too low to detect in mice (data not shown). Moreover, I analyzed levels of HGF that is known to play an important role in driving liver regeneration (Michalopoulos 2007). There was no significant difference in the level of liver HGF between *BubR1*$^{+/+}$ and *BubR1*$^{L/L}$ mice (Fig. 3F).

BubR1 insufficiency increases hepatocyte necrosis accompanied with intercalated disc abnormality.

There were no detectable differences in liver histology between intact *BubR1*$^{+/+}$ and *BubR1*$^{L/L}$ mice (data not shown). In *BubR1*$^{L/L}$ mice, focal hepatic necrosis was observed 12–96 h after PHx and the number of necrotic foci in the liver tissue of *BubR1*$^{L/L}$ mice (2.95±1.11, $p<0.01$) was significantly higher than in the *BubR1*$^{+/+}$ mice (0.23±0.61; Fig. 4A) at 24 h after PHx. Also the necrosis area in *BubR1*$^{L/L}$ mice (0.016±0.005, $p<0.05$) was significantly larger than in the *BubR1*$^{+/+}$ mice (0.010±0.004; Fig. 4B) at 24 h after PHx. The necrosis area in *BubR1*$^{L/L}$ mice showed a maximum at 24 hours and then gradually decreased. The necrotic foci scattered in liver lobule and it was characterized by necrotic hepatocytes and dilation of perisinusoidal spaces with hemorrhage (Fig. 4C, D).

Fig. 4E shows transmission electron microphotographs of hepatic tissue obtained from *BubR1*$^{+/+}$ (panels a1 and a2) and *BubR1*$^{L/L}$ mice (panels b1 and b2) 12 h after PHx. Compared with *BubR1*$^{+/+}$ mice, BubR1$^{L/L}$ mice showed wider intercellular spaces. Observation at higher magnification revealed a wider perisinusoidal space containing atrophic microvilli and dispatched intercalated disks (IDs) (white arrows) in the hepatic tissue of *BubR1*$^{L/L}$ mice (panel b2). In addition, hepatocyte mitochondria were severely swollen and electron-lucent. In *BubR1*$^{L/L}$ mice 12 h after PHx, the number of damaged hepatocytes was higher than in *BubR1*$^{+/+}$ mice, and these features were not observed in *BubR1*$^{L/L}$ mice without PHx (data not shown). These histopathological findings suggest that in *BubR1*$^{L/L}$ mice, abnormal structural intercellular alterations are accompanied by hepatocyte necrosis after PHx.

Effects of low BubR1 expression on desmocollin-1 expression.

To investigate a possible mechanism of liver injury and impaired liver regeneration, I studied the effect of low BubR1 expression on desmocollin-1 (DSC1) expression in mouse liver tissue and HaCaT cells. Immunohistochemical examination revealed that DSC1 expression in the liver was attenuated after PHx in *BubR1* $^{L/L}$ mice compared with *Bub1R*$^{+/+}$ mice (Fig. 5A). Western blot analysis of the liver extracts also revealed that in *BubR1*$^{L/L}$ mice, DSC1 protein expression (0.36±0.18, p<0.05) was significantly decreased 24 h after PHx compared with *BubR1*$^{+/+}$ mice (0.78±0.26) (Fig. 5B). I then examined the effect of BubR1 siRNA on DSC1 expression in HaCaT cells. BubR1 expression was significantly decreased 24 and 48 h after transfection (siRNA(+) vs. siRNA(−) at 24 h; 0.21±0.03 vs. 1.00±0.19, p<0.01, and at 48 h; 0.16±0.05 vs. 0.89±0.25, p<0.01; Fig. 6A). DSC1 mRNA expression was also attenuated and significantly inhibited 48 h after transfection (siRNA(+) vs. siRNA(−); 1.19±0.39 vs. 3.16±0.89, p<0.01; Fig. 6B). These results suggest that BubR1 regulates DSC1 expression in hepatocytes. To demonstrate the effect of BubR1on junctional formation in HaCaT cells treated with and without BubR1 siRNA, I performed confocal laser scanning microscopy analysis using combined BubR1/desmocollin-1/DNA staining. Fig. 6C shows confocal laser microphotographs of HaCaT cells treated with control siRNA (panels a1, a2, a3, and a4) and BubR1 siRNA (panels b1,b2,b3, and b4) 48 h after BubR1 siRNA. Panels a2 and a3 show positive correlation between expression of BubR1 and DSC1. White arrows indicate high expression of BubR1 and DSC1 (panels a2, a3, and a4) in parallel. Yellow arrows indicate low expression of BubR1 and DSC1 (panels a2, a3, a4, b2, b3, and b4) in parallel. Compared with control siRNA (panel a3), BubR1 siRNA (panel b3) showed small number of red dots structure which indicate desmosome junction between cells (orange arrows). These confocal laser scanning microscopy findings suggest that BubR1 expression could correlate with DSC1 expression and affect desmosome junctional formation.

Figure 2. Alterations in BubR1 mRNA expression and liver weight (LW)/body weight (BW) ratio.

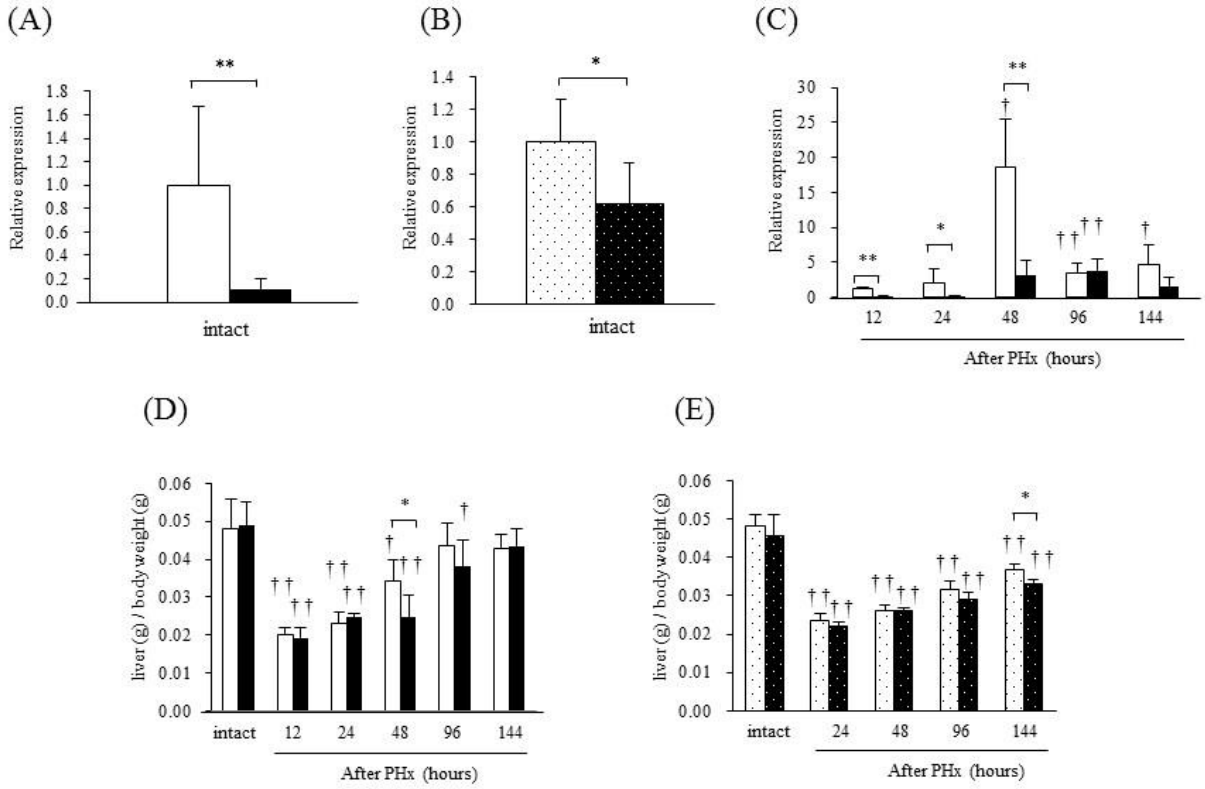

(A) BubR1 mRNA expression in intact *BubR1*$^{+/+}$ (□) and *BubR1*$^{L/L}$ (■) mice. (B) BubR1 mRNA expression in intact 9-week-old (⬚) and 55-week-old (⬛) C57BL/6JJcl mice. (C) Changes in BubR1 mRNA expression in *BubR1*$^{+/+}$ (□) and *BubR1*$^{L/L}$ (■) mice after PHx. Relative expression level to unhepatectomized *BubR1*$^{+/+}$ mice is shown. (D) Changes in LW/BW in *BubR1*$^{+/+}$ (□) and *BubR1*$^{L/L}$ (■) mice after PHx. (E) Changes in LW/BW in 9-week-old (⬚) and 55-week-old (⬛) C57BL/6JJcl mice. Data are presented as the mean ± S.D. †p<0.05, ††p<0.01 vs. intact mouse in each group. *p<0.05, ** p<0.01 vs. *BubR1*$^{+/+}$ mice at each sampling point.

Table 1. Serial change in laboratory data of BubR1$^{+/+}$ and BubR1$^{L/L}$ mice

	BubR1 $^{+/+}$						*BubR1* $^{L/L}$					
		After 70% PHx (hrs)						After 70% PHx (hrs)				
	intact	12	24	48	96	144	intact	12	24	48	96	144
AST (IU/L)	78±28	5202±1539††	1777±1307†	174±72†	82±16	62±9	43±5	7733±1811††*	7006±3134††*	1174±1210	79±17††	61±10†
ALT (IU/L)	42±21	4110±1313††	2044±1188††	179±117	29±6	23±4	22±4	5853±1025††*	4634±2015††*	535±522	29±6	22±3
LDH (IU/L)	359±134	11159±3563††	3497±26734†	376±156	279±40	252±32	248±70	15555±2560††*	14360±8265†*	1880±2015	402±150	307±39*
T-BIL (mg/dL)	0.06±0.01	0.15±0.02††	0.19±0.23	0.12±0.07	0.13±0.07	0.06±0.02	0.10±0.03	0.87±0.92	4.22±2.82†*	5.28±6.97	0.15±0.03†	0.11±0.04*
D-BIL (mg/dL)	0.04±0.02	0.04±0.03	0.10±0.18	0.05±0.04	0.08±0.05	0.02±0.01	0.05±0.01	0.62±0.79	3.26±2.17†*	4.17±5.61	0.05±0.02	0.05±0.01**
I-BIL (mg/dL)	0.02±0.02	0.11±0.02††	0.09±0.05†	0.07±0.04	0.05±0.03	0.05±0.01†	0.06±0.04	0.25±0.13†*	0.96±0.67†*	1.11±1.36	0.10±0.02*	0.06±0.03
TBA (μmol/L)	16.8±31.5	11.6±6.2	24.1±38.1	10.4±6.7	4.7±4.5	2.2±1.0	24.8±47.5	383.8±563.3	1216.2±728.8†*	819.0±905.1	5.2±1.1	3.4±1.3
ALP (IU/L)	469±54	843±188††	921±324††	461±49	308±58††	413±96	482±52	851±437	2725±1231†*	3270±3832	273±96††	328±88†

PHx, partial hepatectomy; AST, asparate: 2-oxoglutarate aminotransferase; ALT, alanine:2-oxoglutarate aminotransferase; LDH, lactate dehydrogenase; T-BIL, total bilirubin; D-BIL, direct bilirubin; I-BIL, indirect bilirubin;TBA, total bile acid; ALP, alkaline phosphatase

† $p<0.05$, † † $p<0.01$ vs each intact, *$p<0.05$, **$p<0.01$ vs *BubR1*$^{+/+}$ mice

Table 2. Serial change in laboratory data of young and old mice.

	young (9-week-old)					aged (55-week-old)				
		After 70% PHx (hrs)					After 70% PHx (hrs)			
	intact	24	48	96	144	intact0	24	48	96	144
AST (IU/L)	30±2	2640±1029††	191±50††	94±16††	77±31	52±28**	5126±1212††*	402±67††**	87±8	71±6
ALT (IU/L)	15±2	2528±728††	169±56†	36±7††	34±15	31±19**	4451±999††*	611±132††**	51±12	28±5
LDH (IU/L)	185±18	6299±3072†	382±70††	527±102††	228±92	305±61*	13592±5059†*	645±60††**	314±5*	325±121

PHx, partial hepatectomy; AST, asparate: 2-oxoglutarate aminotransferase; ALT, alanine:2-oxoglutarate aminotransferase; LDH, lactate dehydrogenase;

T-BIL, total bilirubin; D-BIL, direct bilirubin; I-BIL, indirect bilirubin;TBA, total bile acid; ALP, alkaline phosphatase

† $p<0.05$, † † $p<0.01$ vs each intact, *$p<0.05$, **$p<0.01$ vs young mice

Figure 3. Changes in proliferation markers after PHx.

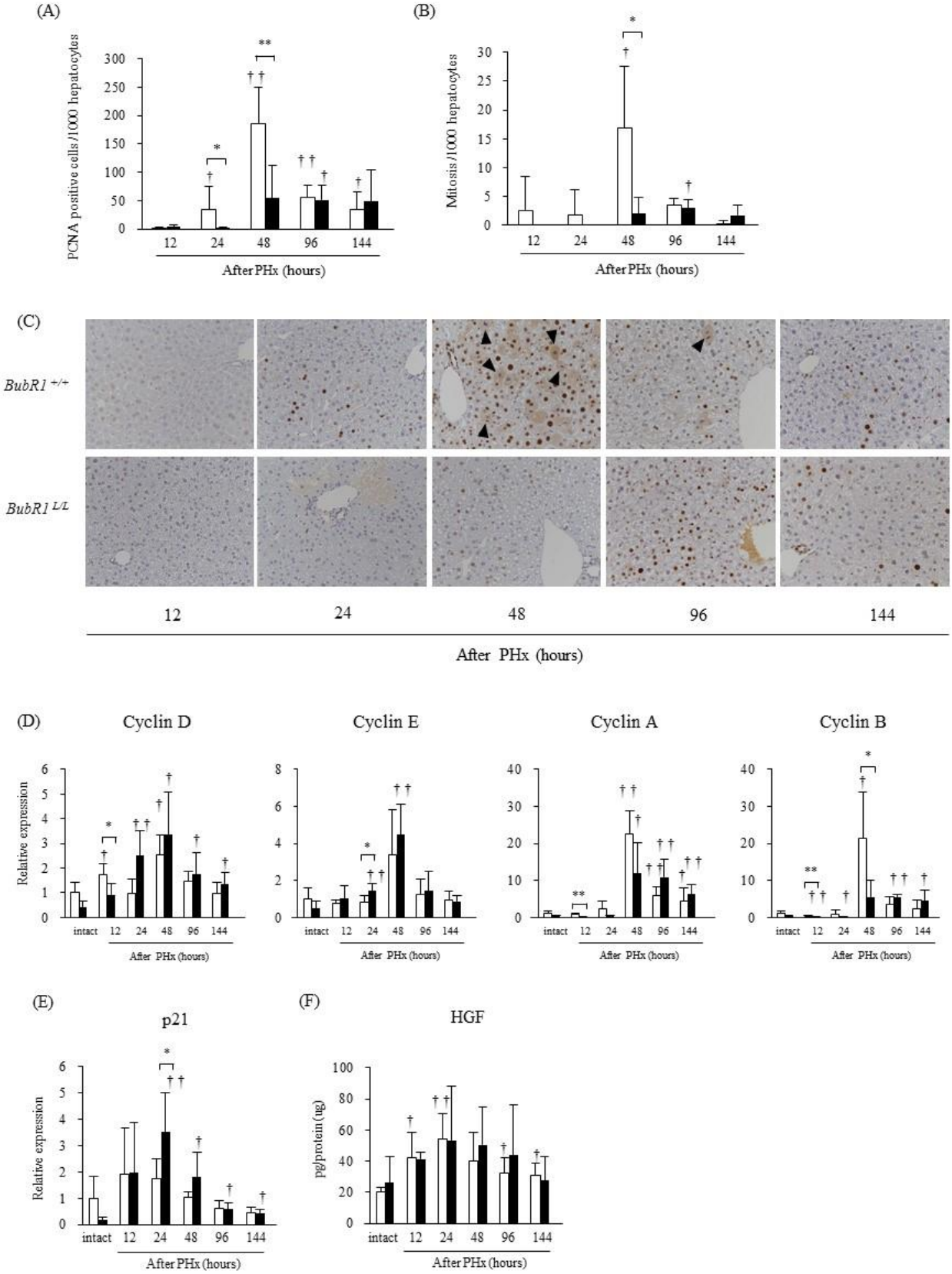

(A) PCNA-positive cells, (B) cells undergoing mitosis. (C) Representative liver sections at 12, 24, 48, 96, 144 hours after PHx stained for PCNA. (magnification ×200): arrowhead, cells undergoing mitosis. (D) cyclin D, cyclin E, cyclin A and cyclin B mRNA expression, (E) p21 mRNA expression, (F) HGF level in *BubR1*$^{+/+}$ (□); *BubR1*$^{L/L}$ (■); data are presented as the mean ± S.D. †p<0.05, ††p<0.01 vs. intact mouse in each group. *p<0.05, ** p<0.01 vs. *BubR1*$^{+/+}$ mice at each sampling point.

Figure 4. Histopathological data.

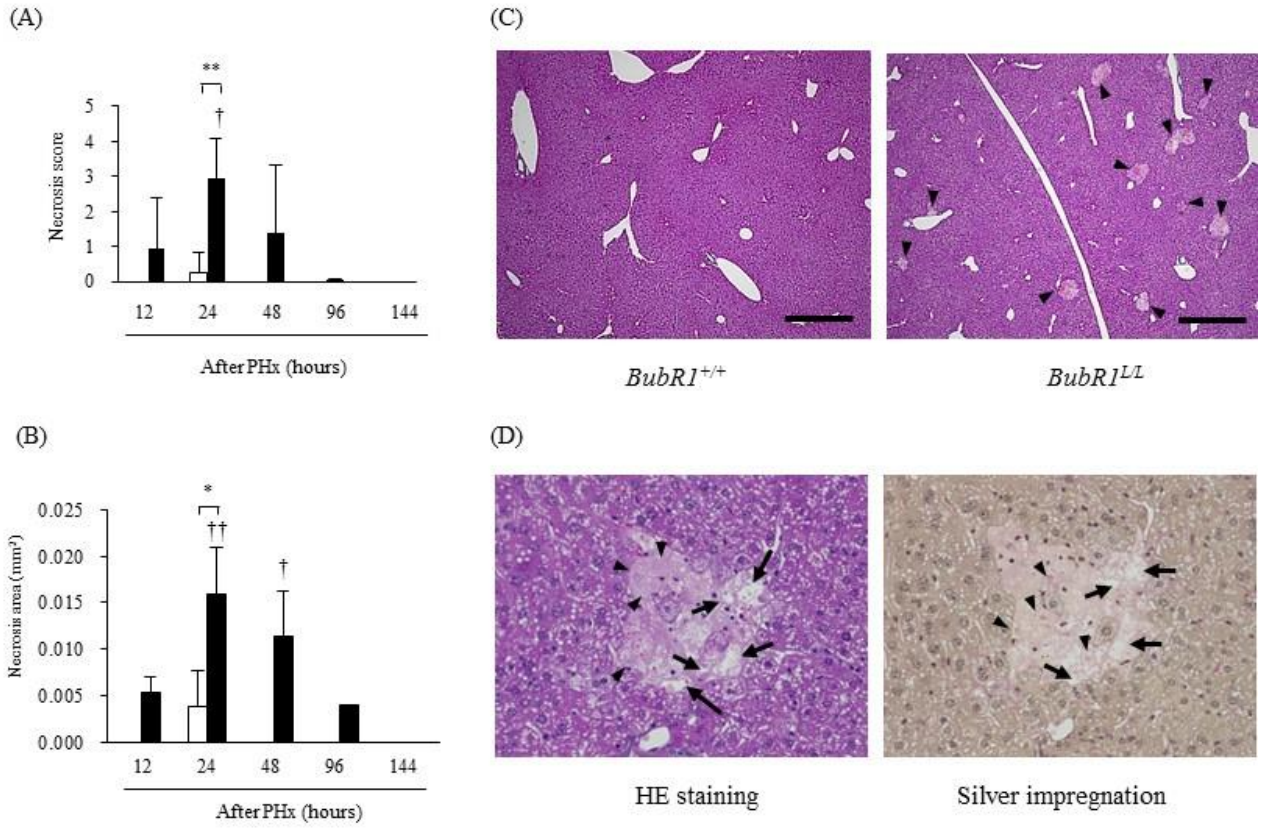

(E)

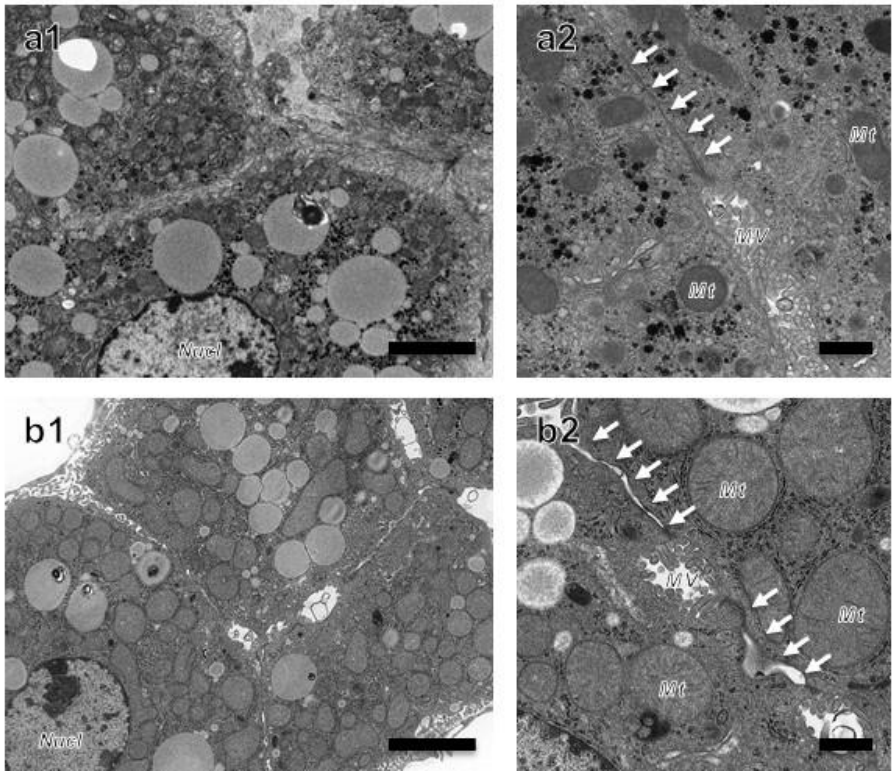

(A) Necrosis score and (B) necrosis area after PHx: *BubR1*$^{+/+}$ (□); *BubR1*$^{L/L}$ (■); data are expressed as the mean ± S.D. †p<0.05, ††p<0.01 vs. 12 h after PHx. **p<0.01 vs. *BubR1*$^{+/+}$ mice at each sampling point. (C) Representative altered liver histopathology at 24 h after PHx with HE staining (magnification ×40): arrowhead, necrosis foci. Scale bars: 500 μm (D) Representative necrosis foci histopathology at 24 h after PHx in *BubR1*$^{L/L}$ mice: Left, HE staining; right, silver impregnation (magnification ×400); arrow, necrotic hepatocytes; arrowhead, dilation of perisinusoidal spaces with hemorrhages. (E) Transmission electron microphotographs of hepatic tissue obtained from *BubR1*$^{+/+}$ (panels a1 and a2) and *BubR1*$^{L/L}$ (panels b1 and b2) mice 12 h after PHx. Compared with *BubR1*$^{+/+}$ mice, *BubR1*$^{L/L}$ mice displayed a wider intercellular space. Observation at higher magnification revealed a wider perisinusoidal space containing atrophic microvilli and dispatched intercalated discs (white arrows) in the hepatic tissue of *BubR1*$^{L/L}$ mice (panel b2). In addition, hepatocyte mitochondria were severely swollen and electron-lucent. Nucl, nucleus; MV, microvilli; Mt, mitochondria; white arrows, intercalated disc. Scale bars: 5 μm in panels a1 and b1; 1 μm in panels a2 and b2

Figure 5. DSC1 expression in hepatocytes after PHx.

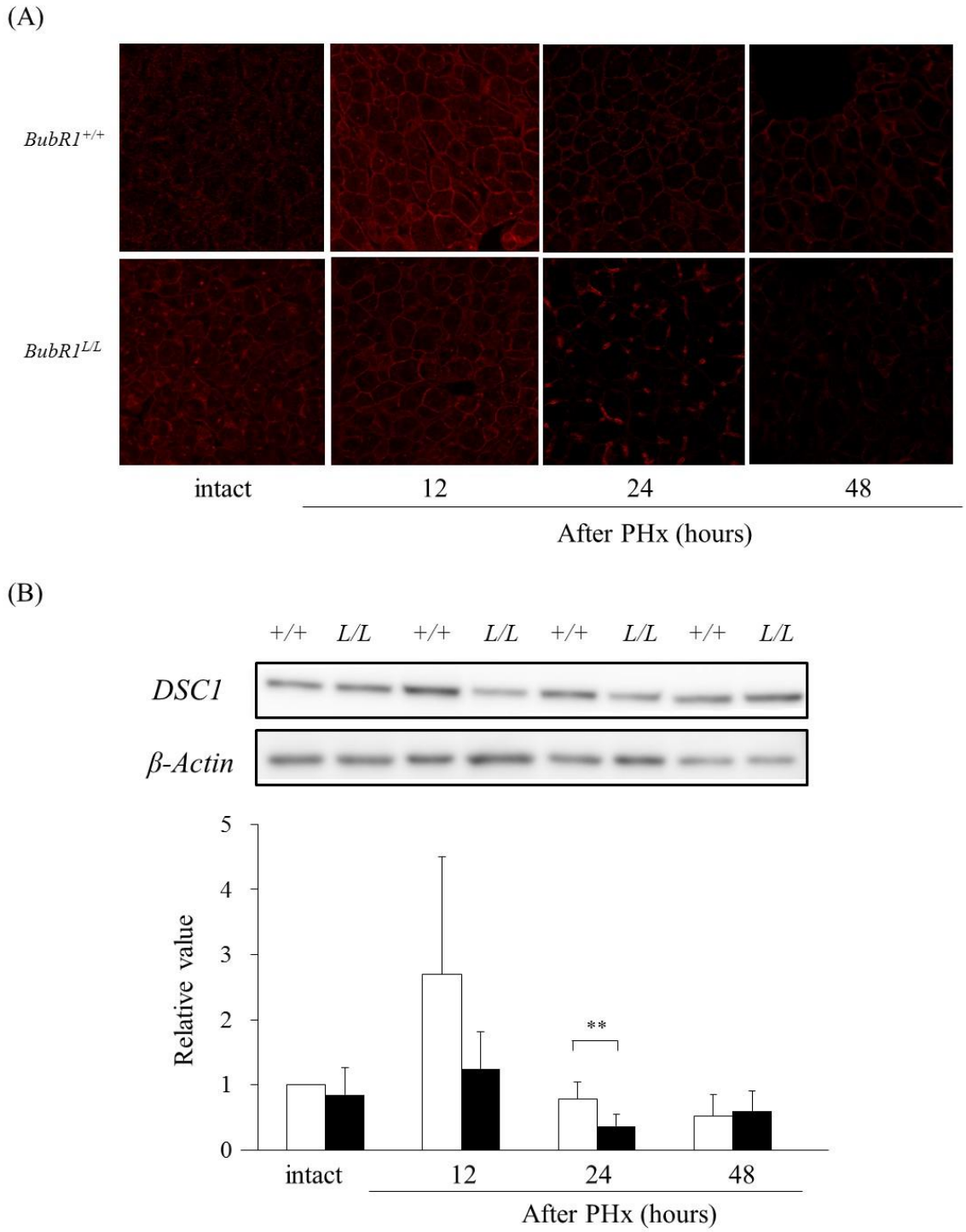

(A) Immunohistochemical staining of DSC1: red staining indicates DSC1 at the intercalated disc. (B) Western blotting data of DSC1: upper panel shows representative data for DSC1; *BubR1*$^{+/+}$ (□); *BubR1*$^{L/L}$ (■); data are mean ± S.D. ***p*<0.01 vs. *BubR1*$^{+/+}$ mice at each sampling point.

Figure 6. Effect of BubR1 siRNA on DSC1 expression in HaCaT3 cells.

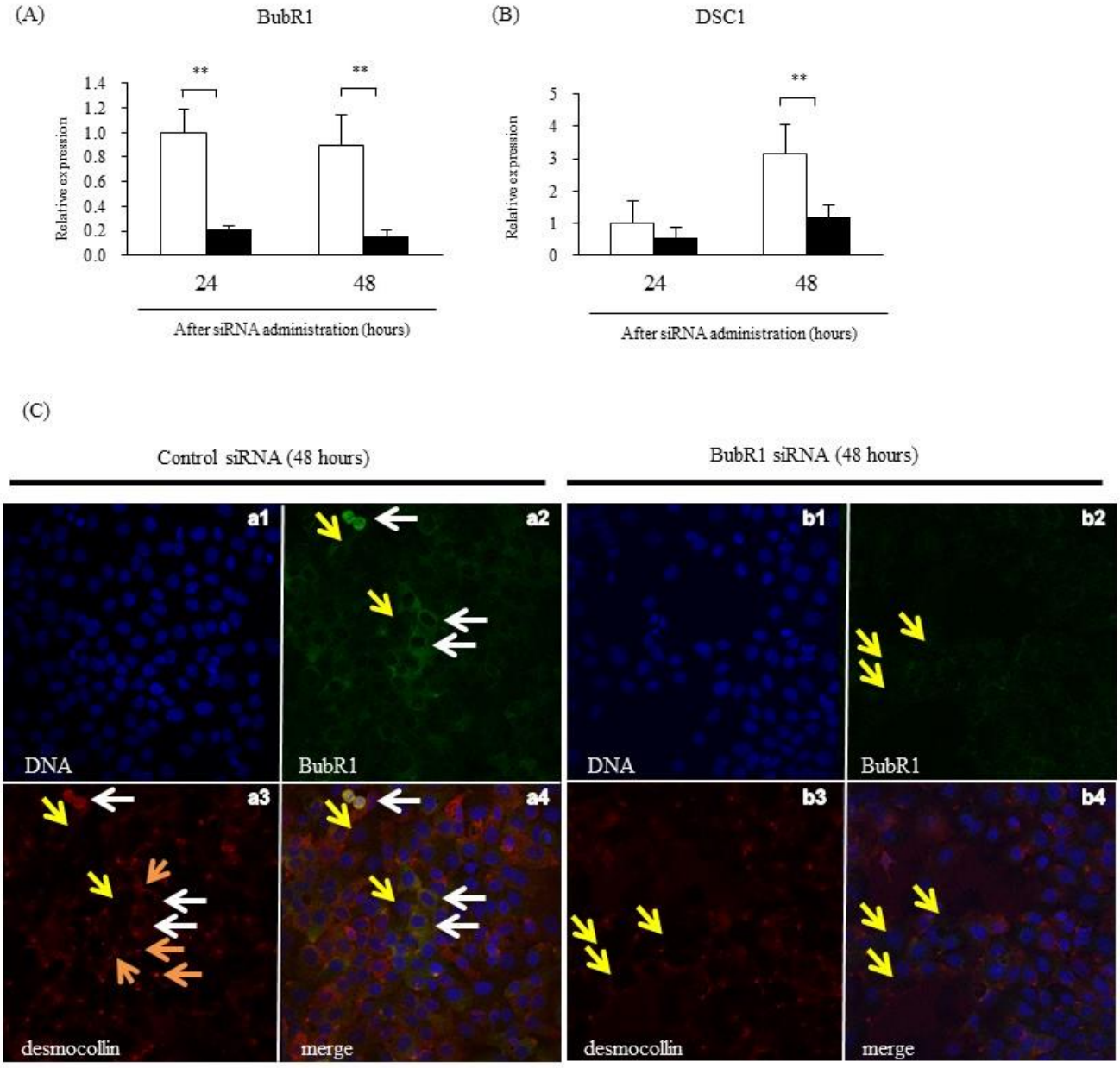

(A) Expression of BubR1 and (B) DSC1 mRNA after BubR1 siRNA transfection; control siRNA (□); BubR1 siRNA (■); data are mean ± S.D. ***p*<0.01 vs. control siRNA at each sampling point.

(C) BubR1 siRNA reduced DSC1 expression and disarrayed HaCaT cells.

Control (panel a1, a2, a3, and a4) and BubR1 siRNA mediated (panel b1, b2, b3, and b4) HaCaT cells were stained using BubR1 (green)- and DSC1-specific antibodies (red) and analyzed by conforcal laser scanning microscopy. DNA was visualized by DAPI staining (blue). Representative

experimental results are shown. White arrows indicate high expression of BubR1 and DSC1. Yellow arrows indicate low expression of BubR1 and DSC1. Compared with control siRNA (panel a3), BubR1 siRNA (panel b3) showed small number of red dots structure which indicate desmosome junction between cells (orange arrows).

Discussion

Aging delays liver regeneration after hepatectomy leading to postoperative liver failure and worsening general condition, which critically affect the patient's prognosis. Although this phenomenon was reported over 50 years ago, the molecular mechanism for the loss of regenerative capacity in aged livers has not been fully elucidated (Timchenko 2009).

Novel findings in this study are summarized as follows: (1) BubR1 insufficiency delays liver regeneration after PHx possibly because of transient impairment of G1-S cell cycle progression; (2) microscopic observation of *BubR1*$^{L/L}$ mice liver shows increased necrotic hepatocytes. Transmission electron microphotographs of hepatic tissue also show increased necrotic hepatocytes accompanied by intercalated disc (ID) abnormality; and (3) I demonstrated, for the first time, that BubR1 controls expression of DSC1, a transmembrane cell adhesion protein in desmosomes. The increase in levels of DSC1, which is expressed in the desmosome, was suppressed in *BubR1*$^{L/L}$ mice liver after PHx. In addition, down-regulation of BubR1 expression with siRNA reduced DSC1 expression in HaCaT cells. These findings provide evidence for a possible molecular mechanism by which aging impairs liver regeneration after hepatectomy.

BubR1 is a key molecule in the spindle assembly checkpoint during mitosis (Yu 2002). Previous studies demonstrated that BubR1 insufficiency in mice caused phenotypic changes that are similar to those found in aging mice (Baker et al. 2004, Matsumoto et al. 2007, Baker et al. 2008, Baker et al. 2011). At the early stage (48 h after PHx) of the liver regeneration, BubR1 mRNA expression was significantly increased in WT mice (*BubR1*$^{+/+}$), suggesting that BubR1 is an important molecule involved in this process. Regeneration assessed by the increased LW/BW after PHx indicates impaired liver regeneration in *BubR1*$^{L/L}$ mice. Aged WT mice also showed impaired liver regeneration, and I observed that BubR1 expression in intact liver significantly decreased in aged mice compared with young mice. These observations indicate that transient delayed liver regeneration after hepatectomy is associated with reduced BubR1 expression and other factor such as EGF and FoxM1B may affect sustained delayed liver regeneration in aged mice (Schmucker et al. 2011). It was previously observed in the senescent liver that activity of ALT, AST, and all types of bilirubin was

increased in the blood of partially hepatectomized aged mice as a result of liver dysfunction (Schmucker 2005). The reduced BubR1 expression level itself did not affect circulating hepatic enzyme levels or liver weight and morphology in untreated *BubR1*$^{L/L}$ mice (data not shown), ruling out the possibility that the reduction of BubR1 expression contributes to alterations of liver function and size in *BubR1*$^{L/L}$ mice (Fig. 1D, Table 1). Thus, my results suggest that age-related inhibition of liver regeneration may be attributed to the reduction in BubR1 expression (Haga et al. 2010, Gregg et al. 2012, Sanchez-Hidalgo et al. 2012).

Hepatocytes are normally quiescent cells. The initiation of hepatocyte proliferation or liver regeneration after hepatectomy requires activation of the mitogenic genes and repression of genes responsible for inhibiting hepatocyte proliferation (Su et al. 2002). Fewer hepatocytes in older animals and humans enter the S-phase after partial hepatectomy compared with younger subjects (Schmucker et al. 2011). In mice, a sharp peak of hepatocyte proliferation is usually observed at 48 h post-PHx (Lehmann et al. 2012), but such steep increase and decrease were not observed in *BubR1*$^{L/L}$ mice. Instead, a few cells initiated proliferation and mitosis 48 h after PHx, and continued to proliferate up to 144 h. These findings suggest that hepatocyte proliferation after PHx was delayed in *BubR1*$^{L/L}$ mice. As a result, delayed cyclin gene expression was observed in hepatectomized *BubR1*$^{L/L}$ mice. Comparison of cyclin-D expression patterns in *BubR1*$^{+/+}$ and *BubR1*$^{L/L}$ mice revealed an apparent delay in cyclin-D induction after PHx in *BubR1*$^{L/L}$ mice. Increasing of cyclin-D and –E expression accelerate the G1/S phase transition (Resnitzky et al. 1994). At 24 h after PHx, cyclin-D and –E expression levels in *BubR1*$^{L/L}$ mice were higher than in *BubR1*$^{+/+}$ mice, it suggested that G1/S phase cells accumulated in *Bub1b*$^{L/L}$ mice. Cyclin-A and -B expression levels increase in late S phase and peak in G2 of normal cells (Muschel et al. 1993). While cyclin-A and -B peak expression levels were observed at 48 h after PHx in *BubR1*$^{+/+}$ mice, moderate cyclin-A and -B expression was induced at 48 h after PHx in *BubR1*$^{L/L}$ mice, and remained constant up to 144 h. These patterns were the same as those of the mitotic and PCNA-positive indices hepatocytes in hepatectomized *BubR1*$^{L/L}$ mice. These results suggested that fewer proliferating hepatocytes may result from a delay in cell cycle progression in *BubR1*$^{L/L}$ mouse hepatocytes. I also found that p21 expression was higher in *BubR1*$^{L/L}$

than *BubR1*$^{+/+}$ mice at 24 h post-PHx. p21 is a CDK inhibitor that hampers the activity of cyclin-E/CDK2 and cyclin-D/CDK4/6 complexes (Wang et al. 2002). Therefore, my results suggest that arrest and/or delay of cell cycle progression from G1 to S phase occurred in hepatocytes in the partially hepatectomized *BubR1*$^{L/L}$ mice. Several studies demonstrate that p21 plays a key role during liver regeneration, such as in the acute liver injury model (Hui et al. 2002) and in the extended hepatectomy model (Lehmann et al. 2012). Moreover there was no difference in the HGF protein content between *BubR1*$^{+/+}$ mice and *BubR1*$^{L/L}$ mice, it suggested that both mice had received the equivalent to the stimulation of cell proliferation. Therefore these studies demonstrated up-regulation of p21 accompanied by a delay in cell cycle progression, which is consistent with my results in *BubR1*$^{L/L}$ mice.

Microscopic observation revealed that after PHx, necrosis but not apoptosis of hepatocytes was strongly induced in *BubR1*$^{L/L}$ mice compared with *BubR1*$^{+/+}$ mice. These observations were consistent with a biochemical analysis of blood in *BubR1*$^{L/L}$ mice. The activities of ALT, AST and all types of bilirubin were increased in partially hepatectomized *BubR1*$^{L/L}$ mice. Such increases are observed in the clinical condition when liver regeneration is impaired in the patients after PHx. In the regenerating liver, epithelial cells require physical contact with extracellular matrix to avoid the detachment induced cell death (DICD) of hepatocytes. After PHx, the reconstitution of a perisinusoidal extracellular matrix stabilizes the newly formed hepatocyte population. Thus, necrosis that is observed in partially hepatectomized *BubR1*$^{L/L}$ mice might be the result of excessive DICD caused by failure of perisinusoidal extracellular matrix reconstitution.

Morphological analysis of livers from *BubR1*$^{L/L}$ mice demonstrated a widened interhepatocyte space, shrinking hepatocytes, a widened perisinusoidal space and atrophy of microvilli in the early stages after PHx, suggesting that partial microstructure failure results from a weak adaptation to changed microcirculatory flow by PHx in *BubR1*$^{L/L}$ mice. Hepatocytes connect via intercellular junctions called IDs to form liver cell plates. IDs are composed of different types of junctional complexes, including gap-junctions made of connexins, tight- and adherens-junctions, and desmosomes. Desmosomes are button-like structures composed of intracellular anchor proteins and

transmembrane adhesion proteins. The intracellular anchor proteins play a role in connecting the cytoskeleton to the transmembrane adhesion proteins including desmocollin, a member of the cadherin family. Desmosomes maintain the integrity of cells to resist mechanical stress, and have dynamic structures whose adhesiveness can switch between high and low affinity adhesive states during cell division, thereby participating in fundamental processes such as cell proliferation, differentiation and morphogenesis (Garrod et al. 2008). Thus, it is possible that the weakened cell attachment observed in the hepatectomized *BubR1*$^{L/L}$ mice could be caused by desmosome abnormality. There are multiple components to hepatocyte junctions. I evaluated expression of occludin located at the tight junctions, E-cadherin located at the adherent junctions, DSC1 and desmoglein in mouse liver. Expression of occludin, E-cadherin, and desmoglein was not so remarkably different between *BubR1*$^{L/L}$ mice and *BubR1*$^{+/+}$ mice by immunohistochemistry (data not shown). Expression of desmocollin-1 was remarkably different in control cells compared with BubR1 reduced cells in *vitro* and in mouse liver. DSC1, a desmosome transmembrane cell adhesion protein, is highly expressed in the liver (Donetti et al. 2004). I showed that up-regulation of DSC1 expression after PHx was not observed in *BubR1*$^{L/L}$ mice. I also demonstrated that small interfering RNA-mediated down-regulation of BubR1 suppressed DSC1 expression in HaCaT cells which is well known that both mRNA and protein are abundant. These results suggest that BubR1 could be a critical regulating factor for DSC1 expression. My hypothesis is that DSC1 could be a target protein which is ubiquitinated by APC/C for the degradation by the proteasome. To investigate this hypothesis, I examined the DSC1 protein expression under APC/C inhibitor by Western blot. Western blot showed that APC/C inhibitor upregulated the DSC1 expression same as securin with which BubR1 directly interacts in *vitro* and in *vivo* (manuscript in preparation). My speculation is that DSC1 is one of the proteins that are ubiquitinated by APC/C and, thus may be one of the targets of BubR1. However, to further explore the relationship between a cell cycle checkpoint protein and a junctional protein are needed. The reduced DSC1 level could cause abnormal cell attachment and delay liver regeneration in *BubR1*$^{L/L}$ mice.

Based on these findings, I propose a possible scenario that occurs after PHx in aged individuals. Hepatectomy induces many stresses, including physical stress and cell division-associated stress. After hepatic resection, portal hypertension occurs because the vascular network in the remnant lobes is reduced despite constant blood flow from the portal vein (Bosch et al. 1992). The liver cells and liver sinusoidal endothelial cell attachment are affected by these stresses during liver regeneration after hepatectomy (Sato et al. 1997), leading to transient DICD and G1 arrest to prevent an excessive DICDs. DSC1 expression also increases, thus leading to reinforcement of desmosomes to maintain cell attachments, which is an important process to prevent massive DICD and anokisis, and thus focal necrosis of hepatocytes. In the case of low BubR1 expression, the increased level of DSC1 expression is not enough to reinforce the desmosome after PHx, leading to increased DICD and anokisis, and thus resulting in hepatocyte focal necrosis. Impairment of cell attachment induces DICD and G1 arrest in a p21-dependent manner (Collins et al. 2005). Therefore, the delayed G1/S progression occurs through up-regulation of p21 caused by secondary effects from the failure of DICD reinforcement because of a DSC1 abnormality, rather than via a direct effect of low BubR1 level. Thus, delayed liver regeneration could occur after PHx in aged patients.

In summary, BubR1 insufficiency causes delayed liver regeneration after partial hepatectomy. BubR1 expression is reduced along with aging. BubR1 insufficiency reduces DSC1 expression in the liver, and thus weakens the microstructural adaptation of the tissue against hepatectomy. BubR1 insufficiency, thus, enhances transient liver failure and injury through the cell cycle delay caused by up-regulation of p21 that results from the weakened microstructural adaptation. Therefore, hepatocyte proliferation is delayed and liver regeneration could be impaired. This work provides new insights into the role of BubR1 in liver regeneration, which may explain worsening liver function after hepatectomy in aged patients.

Chapter 2

Contribution of BubR1 to oxidative stress-induced aneuploidy in p53 deficient cells

Introduction

In 1891, von Hansemann et al. have first observed a numerical chromosome aberration, DNA aneuploidy, in malignant tumors (Hansemann 1891). Previous studies have revealed that significant parts of tumors exhibit DNA aneuploidy and tumors with DNA aneuploidy are significantly correlated with poor cancer prognosis (Cimini 2008). Although extensive efforts have been made to unveil the mechanism causing DNA aneuploidy, it is still not totally understood.

The appropriate expression of spindle assembly checkpoint (SAC) factors may be one important factor to maintain chromosome stability. SAC is a surveillance system controlling the segregation of sister chromatids to daughter cells in mitosis (Musacchio et al. 2007). Overexpression or downregulation of SAC factors may cause an aberrant SAC function, an unequal segregation of chromosomes and DNA aneuploidy (Michel et al. 2001, Wang et al. 2004, Baker et al. 2006, Sotillo et al. 2007, Ando et al. 2010). Consistently, DNA aneuploidy is often found in various tumors with abnormal expression of SAC factors (Perez de Castro et al. 2007).

The p53 signaling pathway is a major suppressor of chromosome instability (Aylon et al. 2011). The p53 controls the transcription of cell cycle checkpoint factors, such as p21, and regulates cell cycle progression at G1-S or G2-M transitions (Levine 1997). The p53 also regulates BubR1 and Mad2 expression and suppresses centrosome amplification (Oikawa et al. 2005, Schvartzman et al. 2011) or aneuploidy. The correlation between abnormal p53 status and DNA aneuploidy has been observed in various human tumors (Ando et al. 2010, Kudela et al. 2012).

Aerobic metabolism, with its advantages of high levels of energy production, is essential for all the organisms exposed to oxidative stress (OS). However, OS causes DNA damage, and is an indirect cause of mutations, gene deletions, and chromosome instability that may lead to malignant transformation. OS is also suggested to contribute to an increase in aneuploid cells (Gorla et al. 2001, Roh et al. 2012). However, how the p53 signaling pathway activated by OS suppresses aneuploidy is not fully understood. In this study, I found that BubR1 and Mad2 are downregulated by OS in p53-dependent manner. When p53 expression was suppressed by siRNA, the BubR1 and Mad2 downregulation by OS was not observed and polyploid cells increased. Importantly, BubR1, but not

Mad2, downregulation suppressed OS-induced polyploidization in p53 knocked down cells, suggesting that BubR1 could have novel function other than SAC to contribute to polyploidization. Moreover, from the analysis of clinical gastric cancer specimens, I found that tumor with positive staining of p53 and high expression of BubR1 tended to exhibit aneuploidy. These findings could provide one possible model for underlying mechanism for gastric carcinogenesis associated with DNA aneuploidy.

Materials and Methods

Reagents and antibodies

Potassium bromate ($KBrO_3$) was purchased from Sigma-Aldrich (Gillingham, UK). The following antibodies were used: a rabbit polyclonal anti-phospho (ser15) p53 antibody (Cell Signaling Technology, Beverly, MA), a mouse monoclonal anti-p53 antibody (DAKO, Dako Cytomation, Glostrup, Denmark), a mouse monoclonal anti-p21 antibody (DAKO, Dako Cytomation, Glostrup, Denmark), a mouse monoclonal anti-BubR1 antibody (Clone 9, BD Transduction Laboratories, San Jose, CA, USA), a mouse monoclonal anti-Mad2 antibody (ImmuQuest, Cleveland, UK), a mouse monoclonal anti-β-actin antibody (Sigma Aldrich, St. Louis, MO, USA), a mouse monoclonal anti-Lamin A/C antibody (Cell Signaling Technology, Beverly, MA), a rat monoclonal anti-α-tubulin antibody (Abcam, Cambridge, UK), an Alexa594-conjugated goat anti-rat IgG antibody and an Alexa488-conjugated goat anti-mouse IgG antibody (Invitrogen, Carlsbad, CA).

Cell culture

Human fibroblasts cells (MRC5) and gastric cancer cells (SNU-1, KATOⅢ) were obtained from ATCC (Manassas, VA, USA). Gastric cancer cells (MKN-45 and MKN-28) were obtained from Riken Cell Bank (Tsukuba, Japan). MRC5 cells were cultured in Eagle's Minimum Essential Medium supplemented with fetal bovine serum (10% v/v), at 37 °C in a 5% CO_2 environment. In my experiments, I used MRC5 cells collected between passages 5 and 8. KATOⅢ, MKN-45 and MKN-28 cells were cultures in Roswell Park Memorial Institute 1640 medium supplemented with fetal bovine serum (10% v/v), at 37 °C in a 5% CO_2 environment.

Western blotting

Cells in the logarithmic growth phase were lysed in lysis buffer (0.5 % NP-40, 20 mM Tris–HCl, pH 8.0, 150 mM NaCl, 1 mM EDTA, and 1 % protease inhibitor cocktail (Nacalai Tesque, Inc., Kyoto, Japan). The protein content was determined using Bradford assay (Bio-Rad, Hercules, CA,

USA). The same amount of protein (8 μg) was loaded on each lane. The immunoreactive bands were detected using the LAS3000 system (GE healthcare, Tokyo, Japan).

Quantification of mRNA in fibroblast cells using real-time PCR

Total RNA was isolated using ISOGEN (Nippongene, Tokyo, Japan) and cDNAs were synthesized from RNAs using SuperScript™ III First-Strand Synthesis SuperMix (Invitrogen, Carlsbad, CA) according to manufacturer's instructions. Quantitative PCR amplification was performed using Applied Biosystems StepOnePlus™ real-time PCR system (Life Technologies, Tokyo, Japan) and a QuantiFast™ SYBR® Green PCR kit (QIAGEN, Hilden, Germany). The *BubR1* and *Mad2* transcript levels were determined using β-actin as an endogenous control. The oligodeoxynucleotide primers were as follows: BubR1, 5′-CTCGTGGCAATACAGCTTCA-3′ (forward) and 5′-CTGGTCAATAGCTCGGCTTC-3′ (reverse)(Ando et al. 2010), Mad2, 5′-ACTTAAATATCTCCCTACCTATACTGAGTCAA-3′ (forward) and 5′-TAGTAACTGTAGATGGAAAAACTTGTGCTA-3′ (reverse) (Bottone et al. 2003) and β-actin, 5′-CCACGAAACTACCTTCAAC--3′ (forward) and 5′-GATCTTCATTGTGCTGGG-3′ (reverse)(Ando et al. 2010).

Small interfering RNA transfection

MRC5 cells were transfected with 10 nmol/L small interfering RNA (siRNA) oligonucleotides using Lipofectamine RNAiMAX Reagent (Invitrogen) according to the manufacturer's instructions. The following siRNA were used: *p53* (5′-GAAAUUUGCGUGUGGAGUA-3′ ON-TARGETplus human TP53 siRNA, Dharmacon), *BubR1* (5′-AAGGGAAGCCGAGCUGUUGAC-3′) (Dai et al. 2004) and Mad2 (SMARTpool: ON-TARGETplus MAD2L1 siRNA, Dharmacon). The ON-TARGETplus Non-targeting Pool (Dharmacon) was used as control. Cells were lysed for Western blotting 24-36 h after transfection.

Fluorescence-activated cell sorting (FACS)

Cells were trypsinized, washed with cold PBS, and fixed with 70% ethanol in PBS at −20 °C. Samples were washed with cold PBS, resuspended in propidium iodide solution (50 μg/ml) containing RNase A (1 mg/ml) and incubated at 37 °C for 30 min. Nuclear DNA content of 10^4 cells were analyzed using FACS calibur system (Becton Dickinson) with CellQuest software (BD Biosciences Japan).

Fluorescence immunostaining

Cells were fixed with 4% paraformaldehyde and immunostained with antibodies against Lamin A/C and α-tubulin. Double staining was done with Alexa488- and Alexa594-conjugated secondary antibodies and the nuclei were counterstained with 4′, 6-diamino-2-phenylindole (DAPI). Images were captured using a BIOREVO BZ-9000 fluorescence microscope (Keyence, Tokyo, Japan). I determined cells as binucleate based on the structure of microtubule and nuclear matrix.

Patients

A total of 182 unselected Japanese patients with primary gastric cancer, who underwent a gastrectomy between 1994 and 2006 at the Department of Surgery and Science, Graduate School of Medical Sciences, Kyushu University Hospital, Fukuoka, were included in this study. None of the patients had been treated preoperatively with cytotoxic drugs. Informed consent was obtained from each patient.

Immunohistochemical staining

Immunohistochemical staining was performed according to a previously described protocol (Ando et al. 2010). Briefly, the sections were placed in 10 mM citrate buffer (pH 6.0) and boiled in a microwave for epitope retrieval. Endogenous peroxidase activity was quenched by incubation in 0.3% H_2O_2. After the blocking with 10% goat serum in PBS, the sections were incubated with a primary antibody. Streptavidin–biotin–peroxidase staining was performed using Histofine SAB-PO (M)

immunohistochemical staining kit (Nichirei, Tokyo, Japan), according to manufacturer's instructions. Sections were counterstained with Mayer's hematoxylin and examined at magnification of 400×.

The p53 expression status was classified by examining immunostaining intensity as previously described (Kakeji et al. 1993, Elledge et al. 1994). A distinct nuclear immunoreactivity for p53 was recorded as positive, and the nuclear staining pattern was usually diffuse. For tumors that showed heterogeneous staining, the predominant pattern was used for scoring. Cases with less than 10% of positively stained cancer cell nuclei were defined as negative, and the rest as positive (Fig.7).

The BubR1 expression status was analyzed by examining immunostaining intensity as previously described (Ando et al. 2010). BubR1 expression level in lymph follicles, which were equally stained in all samples, was assigned an expression score of 1. Weaker staining was assigned score of 0, and samples with stronger staining than that seen in the follicles were given score of 2 (Fig.7).

Analysis of DNA ploidy by Laser scanning cytometry

Nuclear DNA content of gastric cancer samples was measured using laser scanning cytometry (CompuCyte, Westwood, MA, USA) as described previously (Kamada et al. 1997). The samples came from the same paraffin-embedded blocks as those used for immunohistochemical staining. A DNA content histogram was generated and DNA ploidy was determined. DNA index (DI) was calculated according to previously published principles (Furuya et al. 2000). The nuclei were examined after each scan to exclude debris and attached nuclei from the analysis. The DI of G0/G1-phase of lymphocytes or fibroblasts was used as a reference DI = 1.0. Tumors with a DI <1.2 were defined as diploid; DI ≥1.2 or multi-indexed samples were defined as aneuploid.

Statistical analysis

Statistical analysis was performed using the JMP 8.0 statistical software package (SAS Institute, Cary, NC, USA). The Student's *t*-test and Pearson's chi-square test were used wherever appropriate.

Results

OS activated p53 signaling pathway and suppressed the expression of BubR1 and Mad2

Previous studies indicate that p53 could regulate BubR1 expression (Oikawa et al. 2005, Schvartzman et al. 2011). To examine the relationship of OS-activated p53 signaling pathway and BubR1 expression, I cultured human diploid fibroblast MRC5 cells in the presence of oxidant agent $KBrO_3$ for as long as 48 h and analyzed the p53 signaling pathway and BubR1 expression by Western blot. As reported previously (Zhang et al. 2010), both low concentration (0.1 mM) and high concentration (1 mM) of $KBrO_3$ induced phosphorylation of p53 Ser15 and accumulation of p53 and p21 proteins (Fig. 8A). Concomitantly, $KBrO_3$ suppressed BubR1 expression (Fig. 8A). To examine whether reactive oxygen species (ROS) was responsible for these events or not, I added ROS scavenger N-acetylcysteine (NAC) before MRC5 cells were exposed to 0.1 mM $KBrO_3$. Neither $KBrO_3$-induced accumulation of p53 and p21 protein nor decrease of BubR1 protein was observed in the presence of NAC (Fig. 8B). The expression of Mad2, another mitotic checkpoint protein, was also downregulated by $KBrO_3$, (Fig. 8A) and the Mad2 downregulation was also cancelled by NAC (Fig. 8B). These observations indicate that OS activated p53 signaling pathway and suppressed the expression of BubR1 and Mad2 through the action of ROS.

OS-induced downregulation of BubR1 and Mad2 expression was p53 dependent

To examine the relevance of p53 signaling pathway for the decrease of BubR1 and Mad2 expression under OS, I used MRC5 cells in which *p53* had been knocked down by its specific siRNA before exposure to $KBrO_3$. Knockdown of *p53* inhibited p21 protein expression (Fig. 9A). In this condition, the decrease of BubR1 and Mad2 protein under OS was not observed (Fig. 9A). OS-induced downregulation of BubR1 and Mad2 was detected also at mRNA level and *p53* knockdown abrogated *BubR1* and *Mad2* mRNA downregulation (Fig. 9B and 9C). I also observed downregulation of BubR1 by $KBrO_3$ in p53-proficient gastric cancer cell lines (MKN45 cell and SNU-1 cell), but not in p53-mutant or p53-null gastric cancer cell lines (MKN28 cell and KATOⅢ cell) (Fig.10). These

results suggest that the decrease of BubR1 and Mad2 expression under OS was dependent on p53 signaling pathway.

Suppression of BubR1 expression prevent OS-induced polyploidization in p53-depleted cells

Dysfunction of p53 signaling pathway is strongly correlated with aneuploidy (Li et al. 2010). I analyzed the DNA content by FACS of MRC5 cells, which were transfected with *p53* and/or *BubR1* siRNA and exposed to 0.1 mM $KBrO_3$ (Fig.11). SiRNA-mediated downregulation of p53 and BubR1 was confirmed by Western blot (Fig. 11A). In the non-treated or the control siRNA-treated MRC5 cells, polyploid cells (cells with > 4N DNA content) were decreased significantly when cells were cultured in the presence of 0.1 mM $KBrO_3$ ($p < 0.05$) (Fig.11B and 11C-d). These results were probably caused by OS-induced, p53-dependent accumulation of cells in G1 phase and decrease of cells in S to G2/M phase (Fig. 11C-a,b and c). In contrast, when p53 expression was knocked-down by siRNA, neither accumulation in G1 phase, decrease of cells in S to G2/M phase nor decrease of polyploid cells was observed under the same condition (Fig. 11B and 11C). Polyploid cells are usually generated when DNA synthesis occurs without proper cell division. To identify the events for the generation of polyploid cells in the presence of 0.1 mM $KBrO_3$ in p53 knocked-down cells, I observed the nuclear structure of $KBrO_3$-treated cells under the fluorescence microscope. Significant increase of binucleate cells was detected by expouse of $KBrO_3$ in p53 knocked-down cells (Fig.3D and 3E), but not in control siRNA-treated cells (Fig. 11E). When p53 and BubR1 expression was knocked-down at the same time, decrease of cells in S phase and polyploid cells by $KBrO_3$ was observed (Fig. 11C-b and d). Consistently, $KBrO_3$ did not increase binucleate cells in this case (Fig. 11E). In contrast, interestingly, Mad2 knock down did not suppress the emergence of polyploid cells by 0.1 mM $KBrO_3$ in p53-depleted cells (Fig.12). These results indicate that BubR1 could be one of the essential factors of OS-induced polyploidization in p53-depleted cells. My results also suggest that the function of BubR1 required for OS-induced polyploidy might not be related to that of SAC, which is largely mediated by Mad2.

Relationship between p53 and BubR1 expression status, and DNA aneuploidy in gastric cancer specimens

My data from in *vitro* experiments indicate that BubR1 is involved in the OS-induced polyploidization in p53-deficient cells. Polyploid cells are known to result in aneuploidy and promote tumor development (Andreassen et al. 2001, Fujiwara et al. 2005, Roh et al. 2008). To examine whether the correlation among p53 dysfunction, BubR1 expression and OS-induced aneuploidy is observed in clinical tumor specimens or not, I chose gastric cancer, because gastric mucosa is constantly exposed to strong acid and OS might play an important role in gastric organic disorders, including cancer (Suzuki et al. 2012). I immunohistochemically stained p53 and BubR1 in 182 gastric cancer specimens as previously described (Kakeji et al. 1993, Ando et al. 2010) and examined the correlation between them. I regarded p53-positive stained samples as p53 functional loss samples as previously described (Starzynska et al. 1992, Kakeji et al. 1993, Kupryjanczyk et al. 1993, Dix et al. 1994). Among 71 specimens with p53-negative staining, 45 specimens (63.4%) showed high BubR1 expression (score: 1, 2). In contrast, among 111 specimens with p53-positive staining, 95 specimens (85.6%) showed high BubR1 expression ($p < 0.01$; Table 3). These results suggest that BubR1 tends to be highly expressed when p53 function was lost in gastric cancer.

Next, I investigated the relationship between p53/BubR1 expression and DNA aneuploidy in gastric cancer. Using Laser Scanning Cytometer, I have analyzed DNA contents in 77 specimens: 13 specimens with p53-negative staining and low BubR1 expression (score: 0), and 64 specimens with p53-positive staining and high BubR1 expression (score: 1, 2). Among 44 specimens that exhibited aneuploidy, 41 specimens (93.2%) showed p53-positive staining and high BubR1 expression ($p < 0.01$; Table 4). This significant correlation between coexistence of p53 dysfunction and high expression of BubR1 and DNA aneuploidy in gastric cancer may support my results from in *vitro* experiments.

Figure 7. Expression of p53 and BubR1 in gastric cancer.

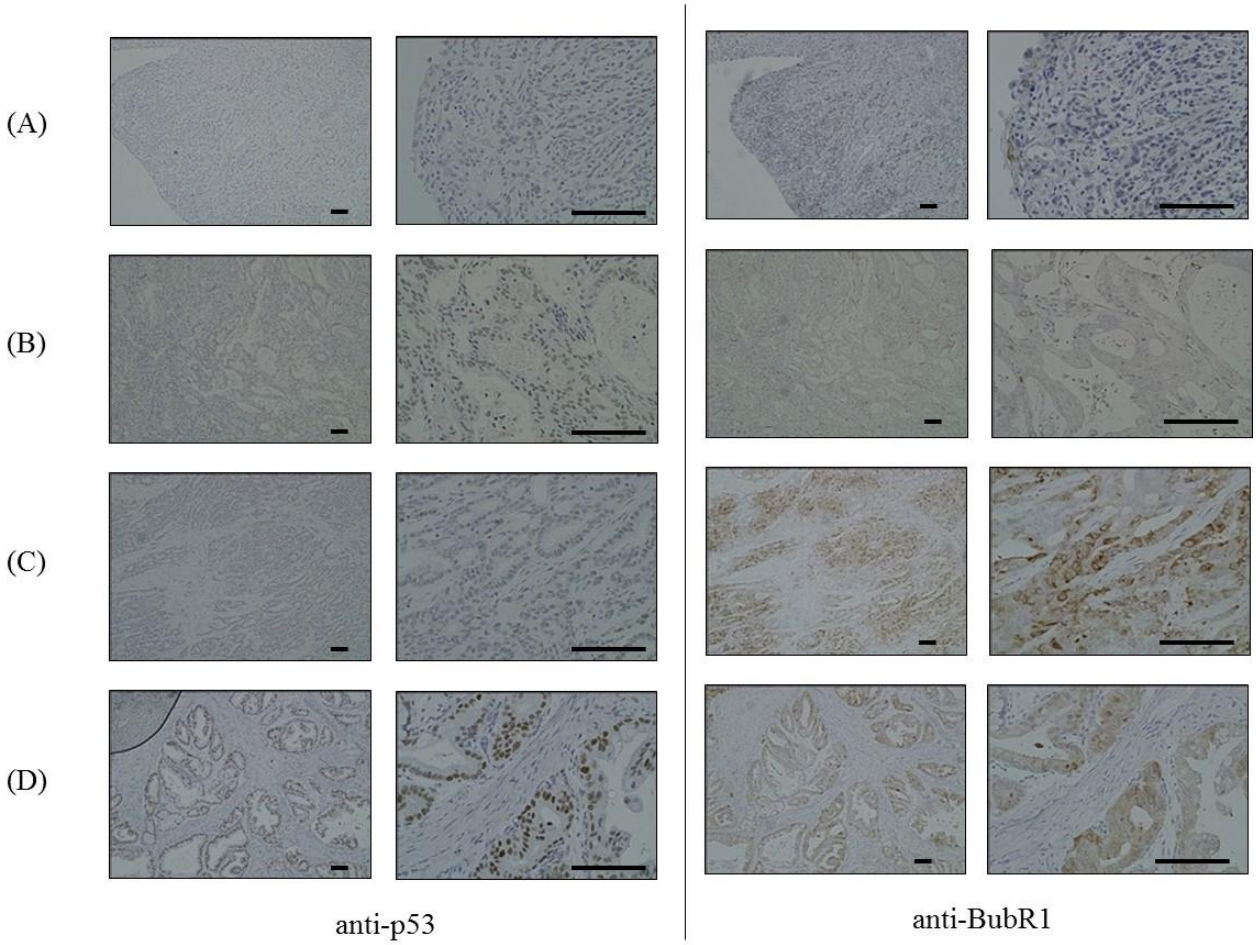

The Immunohistochemical staining figure of four specimens is shown. (Left line: x100, Right line: x400 in magnification) Scale bars, 100 μm. (A) p53-negative staining/ low BubR1 expression (score: 0) specimen (B) p53-negative staining/ high BubR1 expression (score: 1) specimen (C) p53-negative staining/ BubR1 expression (score: 2) specimen (D) p53-positive staining/ BubR1 expression (score: 2) specimen

Figure 8. OS induced p53 signaling pathway and suppressed the expression of BubR1 and Mad2

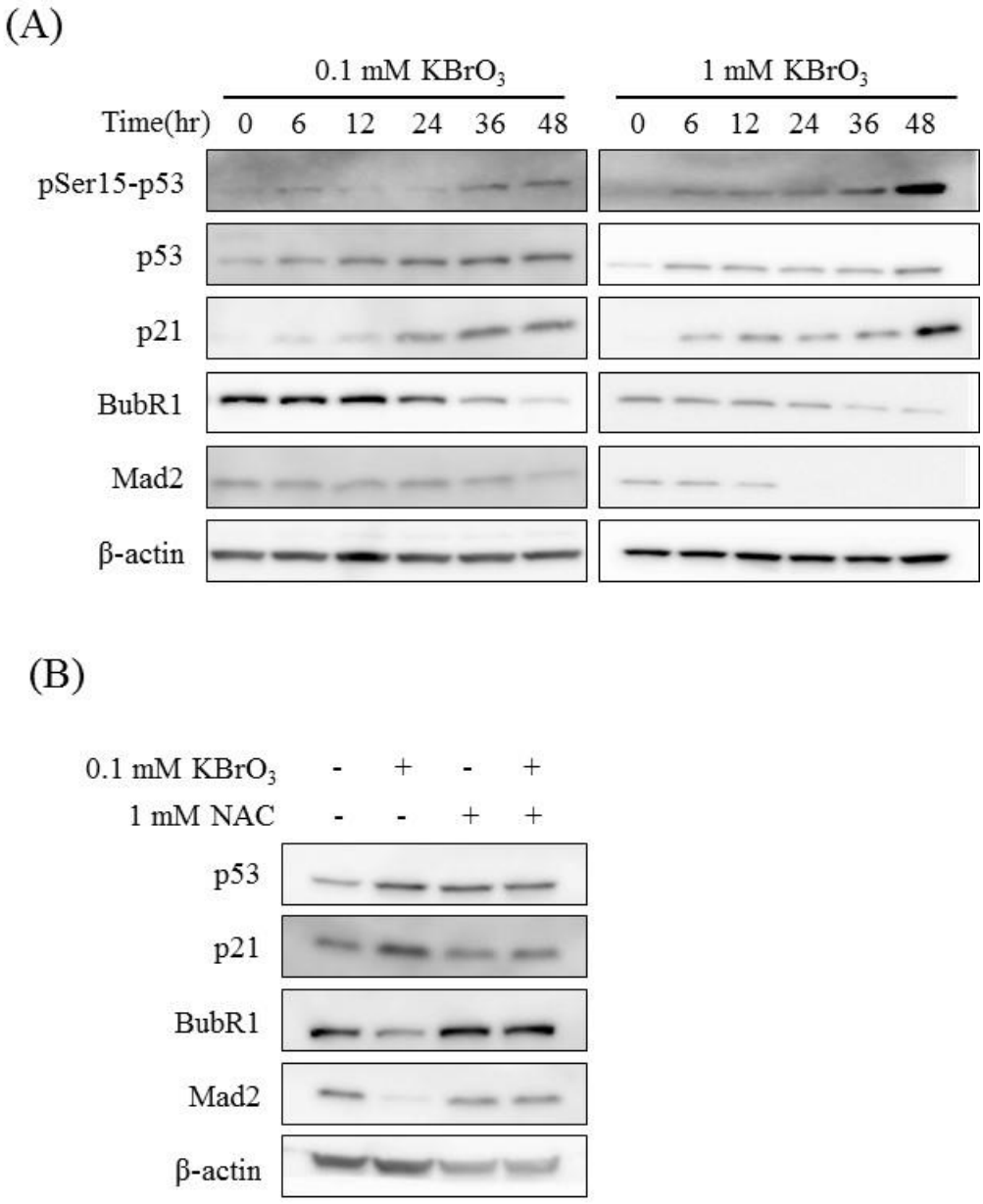

(A) MRC5 cells were exposed to 0.1 or 1mM $KBrO_3$ for 0 to 48 h. Each protein was analyzed by Western blotting. (B) Effect of ROS scavenge on p53 signaling pathway and the expression of BubR1 and Mad2 under OS. MRC5 cells were incubated with 1mM NAC (N-acetylcysteine) prior to $KBrO_3$ treatment for 15min and exposed to 0.1mM $KBrO_3$. After 48h incubation, cells were collected and analyzed by Western blotting. β-actin is shown as a loading control.

Figure 9. OS-induced downregulation of BubR1 and Mad2 expression is p53 dependent.

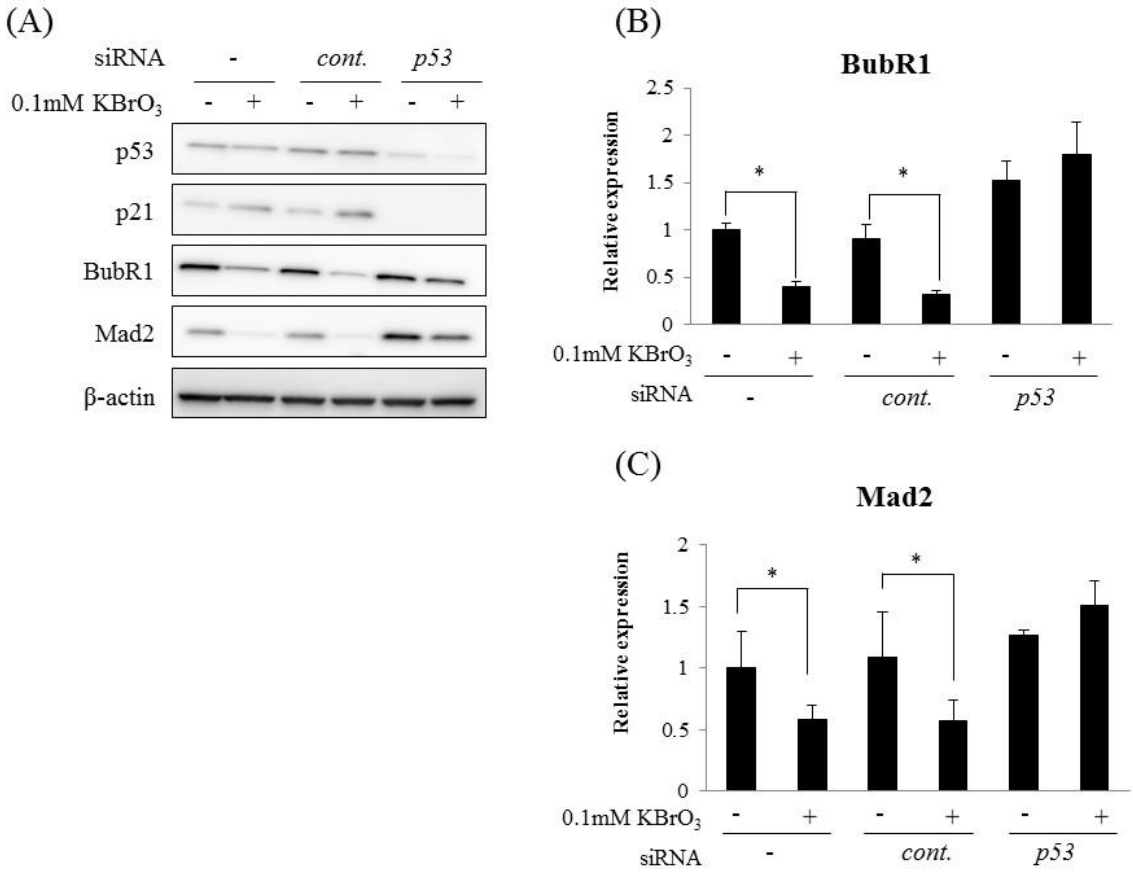

MRC5 cells were transfected with control siRNA or p53 siRNA, and after 24h incubation, 0.1mM $KBrO_3$ was added. (A) Western blot analysis of p53, p21, BubR1 and Mad2 in MRC5 cells after 48h of $KBrO_3$ addition. (B) Relative expression of BubR1 and Mad2 by q-PCR. Knockdown of p53 increased the expression of BubR1 and Mad2 mRNA under OS. The expression scores were normalized to β-actin. Relative expression level to non-transfected under no-OS sample is shown. Data are shown as mean ± S.D. of triplicate measurements. *p<0.05

Figure 10. The response to $KBrO_3$ in gastric cancer cell lines with or without p53 signal dysregulation.

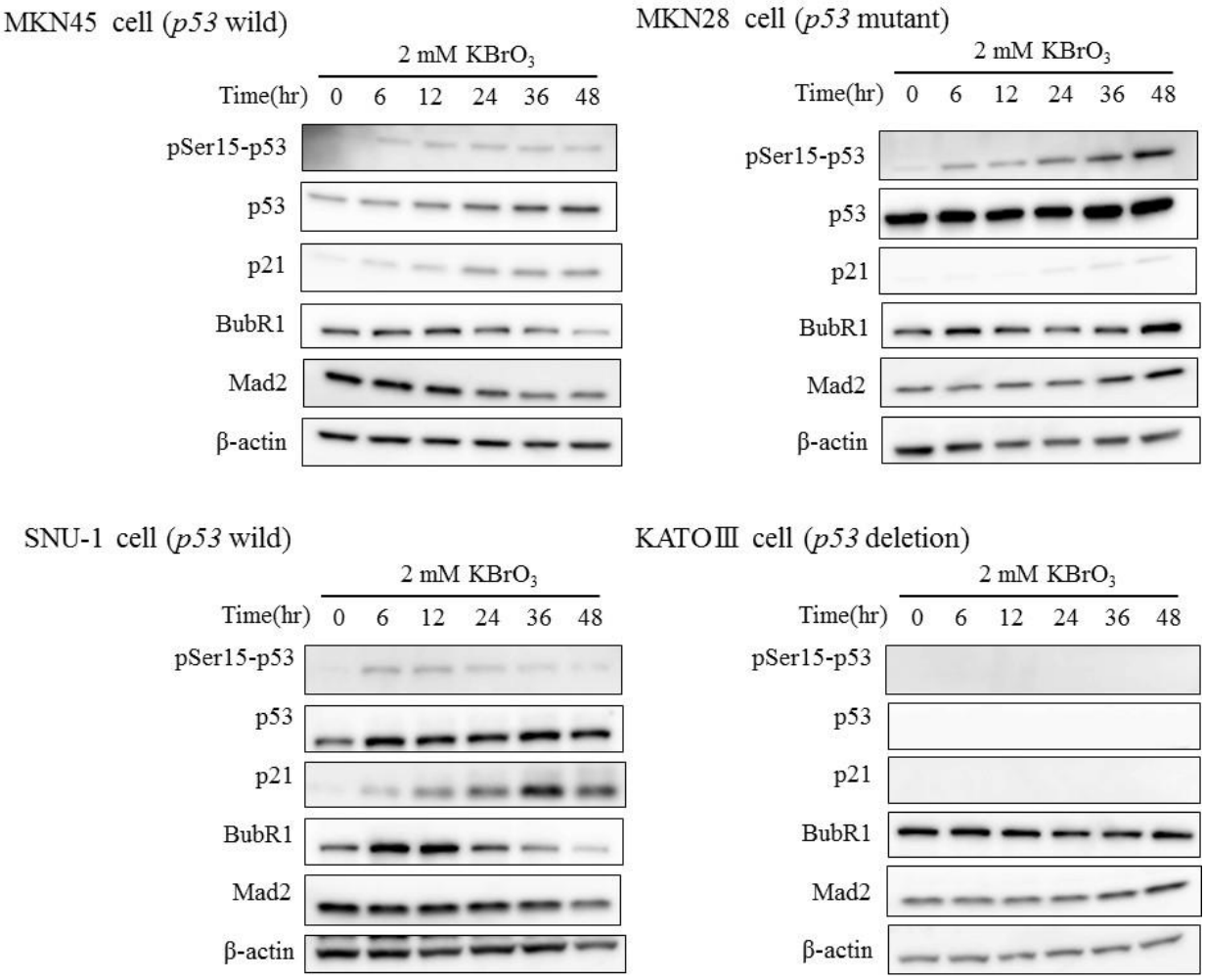

Four gastric cancer cell lines were exposed to 2mM $KBrO_3$ for 0 to 48 h. Each protein was analyzed by Western blotting. In p53-proficient gastric cancer cell lines (MKN45 cell and SNU-1 cell), $KBrO_3$ induced phosphorylation of p53 Ser15 and accumulation of p53 and p21 protein. Concomitantly, $KBrO_3$ suppressed the expression of BubR1. In p53-mutant cell line or p53-null gastric cancer cell lines (MKN28 cell and KATOⅢ cell), the accumulation of p21 proteins were not induced and the decrease of BubR1 expression was not observed by $KBrO_3$ exposure.

Figure 11. Suppression of BubR1 expression prevents OS-induced polyploidization in p53-depleted cells

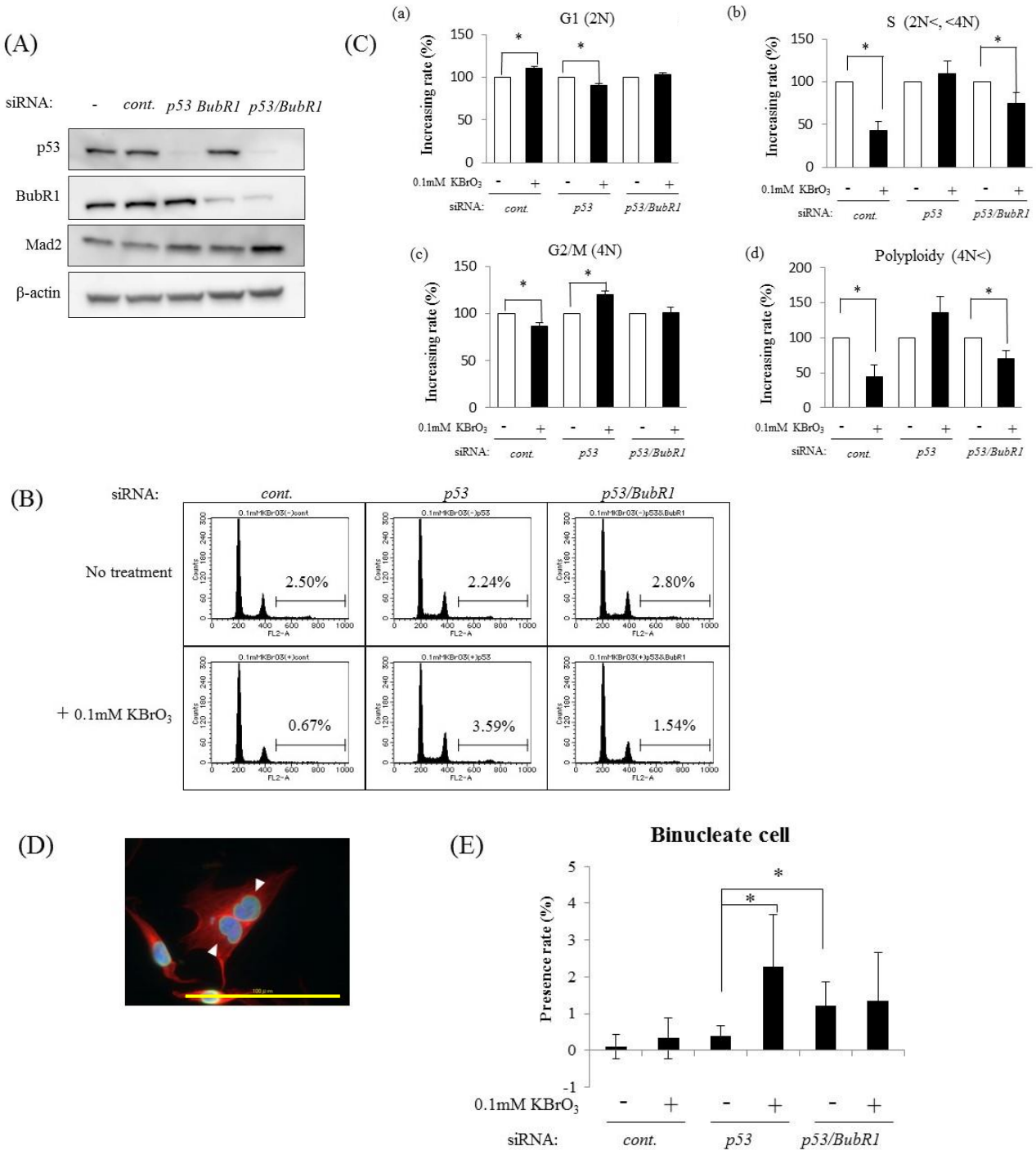

(A) MRC5 cells were transfected with cont. siRNA, p53 siRNA and BubR1 siRNA, and after 36h incubation, siRNA-mediated downregulation of p53 and BubR1 was confirmed by Western blot.

(B) MRC5 cells were transfected with cont. siRNA, p53 siRNA and BubR1 siRNA, and after 36h incubation, 0.1mM $KBrO_3$ was added. Cell cycle distribution and DNA content were analyzed by flow cytometory. Percentage of cells with >4N DNA content is shown. (C) Changes of cells in each cell cycle by 0.1mM $KBrO_3$. Relative percentages of 0.1mM $KBrO_3$-treated cells in G1 phase (2N, a), S phase (2N<, <4N, b), G2/M phase (4N, c) and polyploidy (4N<, d) are shown as filled black bar. * $p<0.05$. Data are shown as mean±S.D. of triplicate measurements. (D) A binucleate cell (nuclei shown by arrowheads) in p53-knockdown MRC5 cells with $KBrO_3$ exposure. Merged immunofluorescence image of α-tubulin (red), Lamin A/C (green) and DAPI (blue) is shown. Scale bar, 100 μm. (E) Percentage of binucleate cells. * $p<0.05$.

Figure 12. Suppression of Mad2 expression dose NOT contribte to prevent OS-induced polyploidization in p53-depleted cells

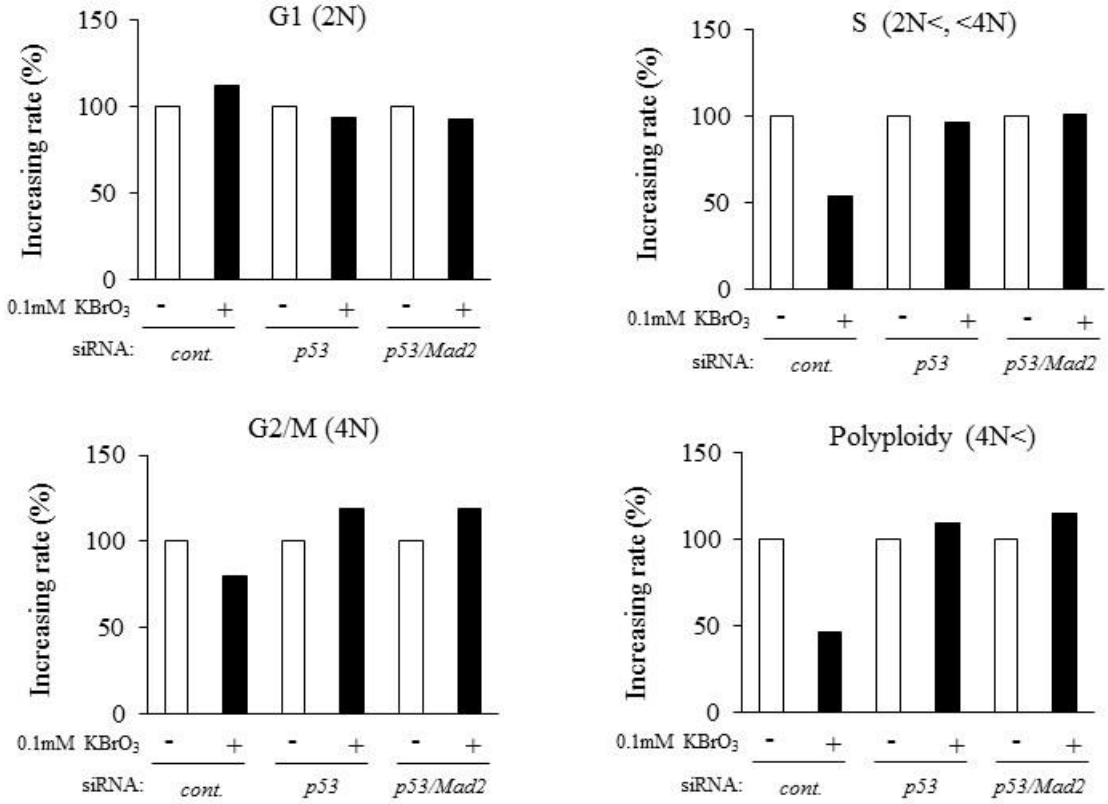

MRC5 cells were transfected with cont. siRNA, p53 siRNA and Mad2 siRNA, and after 36h incubation, 0.1mM $KBrO_3$ was added. Cell cycle distribution. DNA content was analyzed by flow cytometory. Changes of cells in each cell cycle by 0.1mM $KBrO_3$. Relative percentages of 0.1mM $KBrO_3$–treated cells in G1 phase (2N), S phase (2N<, <4N), G2/M phase (4N) and polyploidy (4N<) are shown as filled black bar.

Table 3. P53 expression status and BubR1 expression level in gastric cancer

BubR1 expression level	P53 staining		*p*-value
	Negative	Positive	
Low	26 (36.6)	16 (14.4)	0.0019*
High	45 (63.4)	95 (85.6)	

The values in parentheses are expressed in %. *$p<0.01$

Table 4. DNA ploidy and BubR1/ p53 expression status in gastric cancer

P53/BubR1 status	DNA ploidy		*p*-value
	Diploidy	Aneuploidy	
Negative/ Low	10 (30.3)	3 (6.8)	0.0065*
Positive/ High	23 (69.7)	41 (93.2)	

The values in parentheses are expressed in %. *$p<0.01$

Discussion

It has been proposed that OS might contribute to carcinogenesis by increasing the frequency of genetic mutations, and that the reactive oxygen species, ROS, act as second messengers in multiple intracellular pathways, resulting in malignant transformation (Ralph et al. 2010). Possible models that connect DNA aneuploidy with OS has been proposed (Gorla et al. 2001, Kraniak et al. 2006). However, the role of OS in DNA aneuploidy is still controversial. In my in *vitro* analysis using normal human fibroblast MRC5 cell, when p53 expression was suppressed, OS-producing drug $KBrO_3$ increased polyploid cells, which was partially dependent on sustained expression of BubR1 (Fig. 11). Consistently, I also found that the coexistence of p53 dysfunction and high expression of BubR1 strongly correlated with the extent of aneuploidy in gastric cancer specimens (Table 4).

I found that OS activated the p53 signaling pathway and downregulated the expression of BubR1 and Mad2 (Fig.8). BubR1 and Mad2 downregulation by OS was p53-dependent (Fig.9 and Fig.10). During the activation of SAC, BubR1 and Mad2 form a complex with, Bub3, and Cdc20, and inhibits the proteasome activity of APC/C (Davenport et al. 2006). Accumulation of BubR1 and Mad2 in the absence of functional p53 may cause accumulation of APC/C substrates (Cyclin A/B, Securin, Aurora-A, and Plk1) and may evoke some mitotic errors that induce chromosomal aberrations such as polyploidy (Meraldi et al. 2002, Baek et al. 2003, Incassati et al. 2006, Sotillo et al. 2007). P53 could play a critical role in the repression of OS-initiated mitotic errors through downregulation of SAC factors. In addition, cells lacking p53 function could also have an increased ability to re-enter the cell cycle and initiate DNA replication even in cells with incorrect chromosome number. Such p53 deficiency and SAC accumulation may cause polyploidization and the emergence of cells with > 4N DNA content. Polyploidy is considered pro-tumorigenic as it leads to chromosomal instability that can contribute to tumor development (Fujiwara et al. 2005, Roh et al. 2012). Thus, my results may implicate a novel and critical role of p53 to suppress tumorigenesis associated DNA aneuploidy under OS.

BubR1 knockdown decreased the emergence of polyploid cells significantly under OS in p53-depleted cells (Fig. 11B and 11C-d). Insufficient amount of BubR1 is known to lead to inactivate

SAC function resulting in incidence of DNA aneuploidy (Baker et al. 2004, Matsuura et al. 2006). My result was consistent with these reports in that BubR1 downregulation itself increased binucleate cells in p53-depleted cells in normal culture condition (Fig. 11E). However, my results also suggest that the downregulation of BubR1 suppress the emergence of polyploid cells caused by OS when p53 was suppressed (Fig. 11C-b). Interestingly, downregulation of Mad2 did not suppress the emergence of polyploid cells caused by OS when p53 was suppressed (Fig.12). Currently, the underlying mechanism is still unclear, but recently, as a new role of BubR1 in other than SAC, Baker et al. demonstrated that the reduction in BubR1 levels causes cell senescence by activating the $p16^{Ink4a}$-Rb signaling pathway in mouse model (Baker et al. 2011). Miyamoto et al. also demonstrated that BubR1 is required for ubiquitin-mediated proteasomal degradation of CDC20 in the G0 phase and maintains APC/C^{CDH1} activity (Miyamoto et al. 2011). Such novel function of BubR1 might contribute to the phenotype I observed.

In clinical gastric cancer specimens, I found that BubR1 expression level was strongly correlated with p53 dysfunction (Table 3) and the coexistence of p53 dysfunction and high expression of BubR1 was significantly accompanied with DNA aneuploidy (Table 4). These results suggest that p53 signaling pathway might also regulate BubR1 expression under OS *in vivo* and the failure of this regulation might contribute to the increase of DNA aneuploidy. The increase of OS was observed in aneuploid cells and ROS accumulation could have a role in maintaining aneuploidy formation (Li et al. 2010, Roh et al. 2012). The stomach is a digestive organ subjected to OS directly or indirectly because of the diet, and some gastric organic disorders, including cancer, could be related to such stress (Suzuki et al. 2012). Therefore cumulative effects of OS in aneuploid cells could promote gastric carcinogenesis.

A possible model of gastric carcinogenesis associated with DNA aneuploidy was schematically shown in Fig. 13. When p53 is fully functional, OS does not evoke polyploidization. P53-dependent BubR1 and Mad2 downregulation could be one of the reasons to suppress polyploidization (Fig.13A). In contrast, p53 deficiency may lead to the failure of BubR1 and Mad2 downregulation and accumulated BubR1 or Mad2 could contribute to enhance binucleation and

polyploidization, which will be the trigger of chromosome missegregation and aneuploidy, and, possibly, will promote tumorigenesis (Fig.13B). Importantly, BubR1 downregulation was able to suppress OS-induced binucleation and polyploidization even in p53-depleted cells (Fig.13C), suggesting the possibility for BubR1 as a molecular target for prevention of tumorigenesis through p53 dysfunction and OS-induced aneuploidy. Thus, my findings may have a clinical implication for suppressing gastric carcinogenesis associated with DNA aneuploidy.

Figure 13. A possible model of gastric carcinogenesis associated with DNA aneuploidy

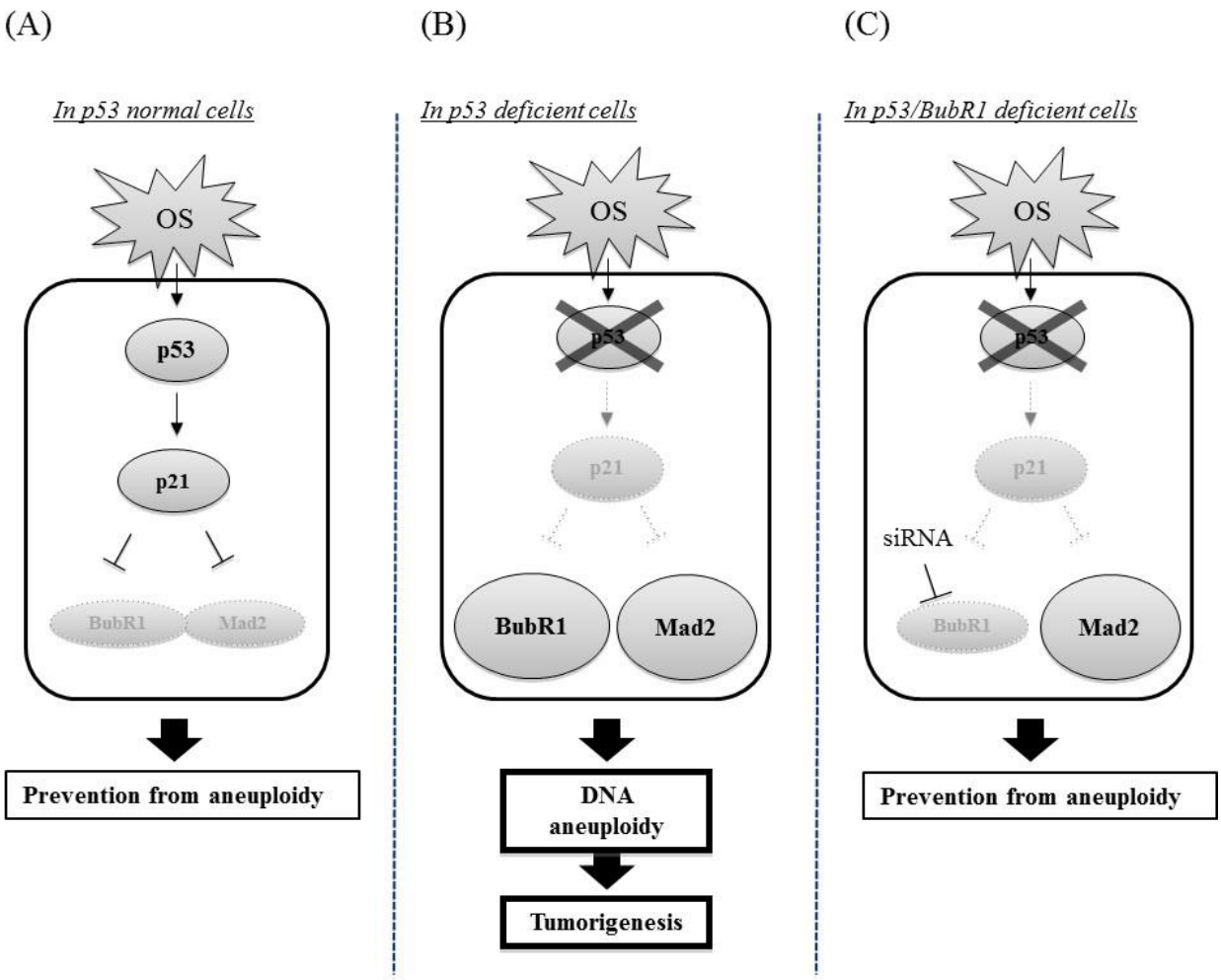

When p53 is fully functional, OS does not envoke polyploidization. P53-dependent BubR1 and Mad2 downregulation could be one of the factors that contribute to suppress polyploidization (A). In contrast, p53 deficiency may lead to the failure of BubR1 and Mad2 downregulation and OS induced aneuploidy (B). BubR1 itself may contribute to enhance OS-induced polyploidization, because siRNA-mediated downregulation of BubR1, but not of Mad2, could suppress OS-induced polyploidization (C). Consistently, coexistence of p53 dysfunction and high expression of BubR1 are frequently observed in gastric cancer specimens with aneuploidy, which suggests the involvement in gastric cancinogenesis associated with DNA aneuploidy.

General Discussion

Mad3/BubR1 was first identified in mutated *S. cerevisiae* in which the cell cycle progressed even after administration of the microtubule polymerization inhibitor benzimidazole (Hoyt et al. 1991), and was demonstrated to play a central role in SAC function (Li et al. 1991, Tang et al. 2001, Musacchio et al. 2007). The SAC function of yeast Mad3 has since been confirmed in homologs in various eukaryotic species (Basu et al. 1998, Cahill et al. 1998, Chen 2002). In tumor cells, the SAC function of BubR1 avoids lethality due to massive chromosome loss (Dorer et al. 2005, Kops et al. 2004). In addition to its SAC function, other functions related to cell division have been reported for BubR1. It determines basal mitotic timing, or the minimum time that elapses between nuclear envelope breakdown and anaphase onset, even when there are no unattached kinetochores (Meraldi et al. 2004). Furthermore, it promotes proper kinetochore-microtubule attachment (Lampson et al. 2005). The multifunctionality of BubR1 has complicated phenotypic interpretation during mitosis. However, when specific mutations that affect only one function but leave the others relatively intact were introduced into BubR1, these functions were shown to be independent (Rahmani et al. 2009). These studies suggest that BubR1 plays an active, multifunctional role in ensuring accurate chromosome separation during mitosis.

As described above, BubR1 localizes to the kinetochore during the mitotic phase and is involved in chromosome division (Musacchio et al. 2007). On the other hand, it has been reported that in several cell lines, BubR1 localizes to the centrosome during interphase and is involved in cilia formation and centrosome replication (Miyamoto et al. 2011, Matsumoto et al. 2009), suggesting that BubR1 has multiple functions during the whole cell cycle. Moreover, BubR1 is revealed to be involved in various cellular phenomena such as cell senescence (Baker et al. 2004), expression of cell adhesion factors, and proliferation of tetraploid cells, the last two of which have been shown in this study, however, which cell cycle each of the phenomena is dependent on is unknown. What is the essential physiological function of BubR1 underlying these multiple functions? I believe that the multifaceted role of BubR1 might be closely related to the function of microtubules. Microtubules are constituents of the cytoskeleton and play a role not only in maintaining and changing the shape of cells, but also in

the transport of substances within cells, formation of cell organelles, cell cycle progression, and cell differentiation (Muroyama et al. 2017, Salogiannis et al. 2017, Werner et al. 2017). Microtubules are hollow cylindrical fibers composed of α/β tubulin heterodimers, and are highly dynamic structures that can stretch and shrink within cells due to polymerization and depolymerization (Fig. 14A). Microtubules are produced at the Microtubule Organizing Center, which is the centrosome in animal cells, and most interstitial microtubules extend radially from the centrosome during interphase (Fig. 14B). Since transport motor proteins move on microtubules, they play an important role in intracellular material transport. Microtubules themselves can cause cell cycle-dependent morphological changes (Fig. 14C). Cilia/flagella are organelles composed of microtubules and are formed during G0/G1 phase. Cilia/flagella withdraw when cells enter S phase, following which centrosome replication occurs and the microtubule network is restructured. For subsequent chromosome division, the duplicated centrosomes move to the two poles of the cell, nucleating microtubules, which bundle to form the mitotic spindle. The spindles capture the chromosomes, bind kinetochores and microtubules, and pull the chromosomes apart, using well-organized system. I noticed that this cell cycle-dependent microtubule change overlaps with the cellular phenomenon involving BubR1 (Izumi et al. 2009, Lampson et al. 2005, Musacchio et al. 2007, Miyamoto et al. 2011)(Fig. 14B, C). In addition, the mechanism of cellular senescence due to cilia dysplasia has been reported (Li et al. 2011, Inoko et al. 2012), highlighting the possibility that cellular senescence induced by the low expression of BubR1 is caused by ciliary dysplasia. Further, it has been reported that in the course of cell differentiation, the expression level of the cell adhesion factor is regulated depending on microtubule transport (Lechler et al. 2007). The suppression of DSC1 expression due to the low expression of BubR1 is also considered to be mediated by the transport function of microtubules. Therefore, I believe that the essential physiological function of BubR1 might be to maintain homeostasis in microtubule function. In the future, I would like to work to verify this hypothesis and investigate the influence of BubR1 on the signals required for cell cycle-dependent microtubule changes and the factors related to microtubule transport.

Figure 14. Microtubule function and BubR1 involvement

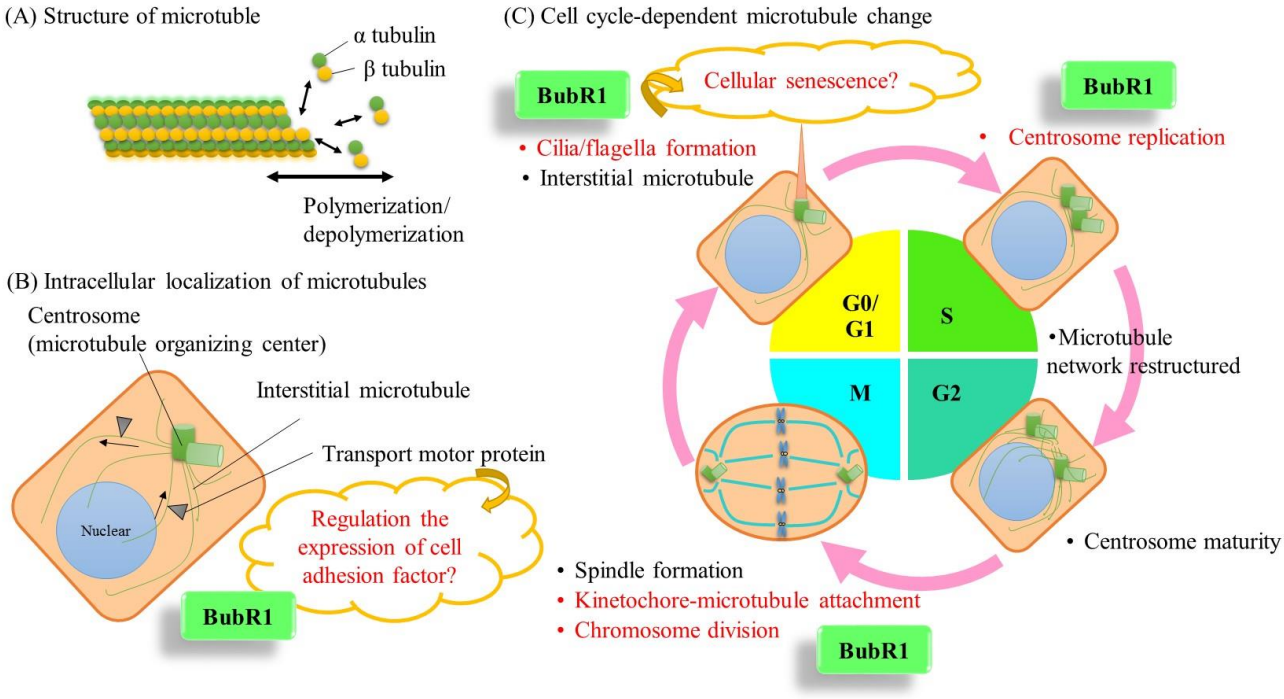

(A) Microtubules are hollow cylindrical fibers composed of α/β tubulin heterodimers, and are highly dynamic structures that can stretch and shrink within cells due to polymerization and depolymerization. (B) Microtubules are produced at the Microtubule Organizing Center, which is the centrosome in animal cells, and most interstitial microtubules extend radially from the centrosome during interphase. Transport motor proteins move on microtubules, they play an important role in intracellular material transport. (C) Microtubules cause cell cycle-dependent morphological changes. Red letters are the cellular phenomenon in which the involvement of BubR1are reported or are suggested.

In addition to MVA/PCS syndrome, which is caused by insufficient BubR1 expression and SAC dysfunction (Hanks et al. 2004, Matsuura et al. 2006), various diseases have been linked to BubR1 functions, such as senescence through the dysregulation of $p16^{Ink4a}$ expression (Baker et al. 2008, Baker et al. 2011) and impaired ciliogenesis through abnormal APC/C-CDH1 activation (Miyamoto et al. 2011). I investigated the physiological relevance of BubR1 in liver regeneration using mice expressing low levels of BubR1, and discovered a novel function for BubR1 in the regulation of DSC1 expression. Delay of liver regeneration due to aging and hepatic disorders may have been caused by abnormal DSC1 expression due to BubR1 insufficiency.

Since various diseases are associated with low BubR1 expression, increasing its expression might have therapeutic potential. However, this approach may increase the risk of carcinogenesis, as high BubR1 expression with p53 dysfunction may lead to cell proliferation and tumor growth. There are numerous reports that high levels of BubR1 may be a prognostic marker for tumor recurrence and disease progression (Yuan et al. 2006, Burum-Auensen et al. 2007, Yamamoto et al. 2007). The development of inhibitors that target the C-terminal kinase domain of BubR1 is underway, but side effects are predicted due to lack of specificity (Kapanidou et al. 2015). Unfortunately, no drug targeting BubR1 itself has been successfully developed. Therefore, targeting the factors affecting each function downstream of BubR1 may be more desirable to produce safer drugs.

Despite the discovery of several SAC-independent functions for BubR1, examination of the relationships between the various functions of BubR1 has not been performed. It remains unknown whether these functions are independent or correlated with each other, or whether the presence and absence of essential regions of BubR1 are important for multiple functions. Structure-function studies to locate the specific regions in BubR1 upon which each function depends will be necessary. Further clarification of the interplay between different BubR1 functions at the molecular level will lead to the elucidation of new disease mechanisms related to BubR1, and contribute to the development of effective treatments for BubR1-related diseases.

Acknowledgements

I thank Prof. Genzou Takemura, Department of Internal Medicine Asahi University School of Dentistry, for professional comments on the electron microphotographs, Junji Kishimoto, Department of Research and Development of Next Generation Medicine Faculty of Medical Sciences, Kyushu University, for statistical advice, and Makoto Iimori, Molecular Oncology Graduate School of Medical Sciences, Kyushu University, for valuable comments and critical reading of the manuscript.

References

Ando, K., Y. Kakeji, H. Kitao, M. Iimori, Y. Zhao, R. Yoshida, E. Oki, K. Yoshinaga, T. Matumoto, M. Morita, Y. Sakaguchi and Y. Maehara (2010). "High expression of BUBR1 is one of the factors for inducing DNA aneuploidy and progression in gastric cancer." Cancer Sci **101**(3): 639-645.

Andreassen, P. R., O. D. Lohez, F. B. Lacroix and R. L. Margolis (2001). "Tetraploid state induces p53-dependent arrest of nontransformed mammalian cells in G1." Mol Biol Cell **12**(5): 1315-1328.

Aylon, Y. and M. Oren (2011). "p53: guardian of ploidy." Mol Oncol **5**(4): 315-323.

Baek, K. H., H. J. Shin, J. K. Yoo, J. H. Cho, Y. H. Choi, Y. C. Sung, F. McKeon and C. W. Lee (2003). "p53 deficiency and defective mitotic checkpoint in proliferating T lymphocytes increase chromosomal instability through aberrant exit from mitotic arrest." J Leukoc Biol **73**(6): 850-861.

Baker, D. J., K. B. Jeganathan, J. D. Cameron, M. Thompson, S. Juneja, A. Kopecka, R. Kumar, R. B. Jenkins, P. C. de Groen, P. Roche and J. M. van Deursen (2004). "BubR1 insufficiency causes early onset of aging-associated phenotypes and infertility in mice." Nat Genet **36**(7): 744-749.

Baker, D. J., K. B. Jeganathan, L. Malureanu, C. Perez-Terzic, A. Terzic and J. M. van Deursen (2006). "Early aging-associated phenotypes in Bub3/Rae1 haploinsufficient mice." J Cell Biol **172**(4): 529-540.

Baker, D. J., C. Perez-Terzic, F. Jin, K. S. Pitel, N. J. Niederlander, K. Jeganathan, S. Yamada, S. Reyes, L. Rowe, H. J. Hiddinga, N. L. Eberhardt, A. Terzic and J. M. van Deursen (2008). "Opposing roles for p16Ink4a and p19Arf in senescence and ageing caused by BubR1 insufficiency." Nat Cell Biol **10**(7): 825-836.

Baker, D. J., T. Wijshake, T. Tchkonia, N. K. LeBrasseur, B. G. Childs, B. van de Sluis, J. L. Kirkland and J. M. van Deursen (2011). "Clearance of p16Ink4a-positive senescent cells delays ageing-associated disorders." Nature **479**(7372): 232-236.

Baker, K. and P. L. Beales (2009). "Making sense of cilia in disease: the human ciliopathies." Am J Med Genet C Semin Med Genet **151c**(4): 281-295.

Basu, J., E. Logarinho, S. Herrmann, H. Bousbaa, Z. Li, G. K. Chan, T. J. Yen, C. E. Sunkel and M. L. Goldberg (1998). "Localization of the Drosophila checkpoint control protein Bub3 to the kinetochore requires Bub1 but not Zw10 or Rod." Chromosoma **107**(6-7): 376-385.

Bolanos-Garcia, V. M. and T. L. Blundell (2011). "BUB1 and BUBR1: multifaceted kinases of the cell cycle." Trends Biochem Sci **36**(3): 141-150.

Bosch, J., P. Pizcueta, F. Feu, M. Fernandez and J. C. Garcia-Pagan (1992). "Pathophysiology of portal hypertension." Gastroenterol Clin North Am **21**(1): 1-14.

Bottone, F. G., Jr., J. M. Martinez, J. B. Collins, C. A. Afshari and T. E. Eling (2003). "Gene modulation by the cyclooxygenase inhibitor, sulindac sulfide, in human colorectal carcinoma cells: possible link to apoptosis." J Biol Chem **278**(28): 25790-25801.

Burum-Auensen, E., P. M. De Angelis, A. R. Schjolberg, K. L. Kravik, M. Aure and O. P. Clausen (2007). "Subcellular localization of the spindle proteins Aurora A, Mad2, and BUBR1 assessed by immunohistochemistry." J Histochem Cytochem **55**(5): 477-486.

Cahill, D. P., C. Lengauer, J. Yu, G. J. Riggins, J. K. Willson, S. D. Markowitz, K. W. Kinzler and B. Vogelstein (1998). "Mutations of mitotic checkpoint genes in human cancers." Nature **392**(6673): 300-303.

Chen, R.-H. (2002). "BubR1 is essential for kinetochore localization of other spindle checkpoint proteins and its phosphorylation requires Mad1." J Cell Biol **158**(3): 487-496.

Cimini, D. (2008). "Merotelic kinetochore orientation, aneuploidy, and cancer." Biochim Biophys Acta. **1786**(1): 32-40.

Collins, N. L., M. J. Reginato, J. K. Paulus, D. C. Sgroi, J. Labaer and J. S. Brugge (2005). "G1/S cell cycle arrest provides anoikis resistance through Erk-mediated Bim suppression." G1/S cell cycle arrest provides anoikis resistance through Erk-mediated Bim suppression Mol Cell Biol **25**(12): 5282-5291.

Dai, W., Q. Wang, T. Liu, M. Swamy, Y. Fang, S. Xie, R. Mahmood, Y. M. Yang, M. Xu and C. V. Rao (2004). "Slippage of mitotic arrest and enhanced tumor development in mice with BubR1 haploinsufficiency." Cancer Res **64**(2): 440-445.

Davenport, J., L. D. Harris and R. Goorha (2006). "Spindle checkpoint function requires Mad2-dependent Cdc20 binding to the Mad3 homology domain of BubR1." Exp Cell Res **312**(10): 1831-1842.

Dix, B., P. Robbins, S. Carrello, A. House and B. Iacopetta (1994). "Comparison of p53 gene mutation and protein overexpression in colorectal carcinomas." Br J Cancer **70**(4): 585-590.

Donetti, E., E. Boschini, A. Cerini, S. Selleri, C. Rumio and I. Barajon (2004). "Desmocollin 1 expression and desmosomal remodeling during terminal differentiation of human anagen hair follicle: an electron microscopic study." Exp Dermatol **13**(5): 289-297.

Dorer, R. K., S. Zhong, J. A. Tallarico, W. H. Wong, T. J. Mitchison and A. W. Murray (2005). "A Small-Molecule Inhibitor of Mps1 Blocks the Spindle-Checkpoint Response to a Lack of Tension on Mitotic Chromosomes." Curr Biol **15**(11): 1070-1076.

Duncan, A. W., M. H. Taylor, R. D. Hickey, A. E. Hanlon Newell, M. L. Lenzi, S. B. Olson, M. J. Finegold and M. Grompe (2010). "The ploidy-conveyor of mature hepatocytes as a source of genetic variation." Nature **467**(7316): 707-710.

Elledge, R. M., G. M. Clark, S. A. Fuqua, Y. Y. Yu and D. C. Allred (1994). "p53 protein accumulation detected by five different antibodies: relationship to prognosis and heat shock protein 70 in breast cancer." Cancer Res **54**(14): 3752-3757.

Fausto, N., J. S. Campbell and K. J. Riehle (2006). "Liver regeneration." Hepatology **43**(2 Suppl 1): S45-53.

Fausto, N. & Webber, E. M. (1994) The Liver Biology and Pathobiology (eds Arias, I. M., Boyer, J. L., Fausto, N., Jacoby, W. B., Schachter, D., Shafritz, D.A.) (Raven Press Ltd, New York, USA) 53–68.

Fortner, J. G. and R. M. Lincer (1990). "Hepatic resection in the elderly." Ann Surg **211**(2): 141-145.

Fujiwara, T., M. Bandi, M. Nitta, E. V. Ivanova, R. T. Bronson and D. Pellman (2005). "Cytokinesis failure generating tetraploids promotes tumorigenesis in p53-null cells." Nature **437**(7061): 1043-1047.

Furuya, T., T. Uchiyama, T. Murakami, A. Adachi, S. Kawauchi, A. Oga, T. Hirano and K. Sasaki (2000). "Relationship between chromosomal instability and intratumoral regional DNA ploidy heterogeneity in primary gastric cancers." Clin Cancer Res **6**(7): 2815-2820.

Garrod, D. and M. Chidgey (2008). "Desmosome structure, composition and function." Biochim Biophys Acta **1778**(3): 572-587.

Gorla, G. R., H. Malhi and S. Gupta (2001). "Polyploidy associated with oxidative injury attenuates proliferative potential of cells." J Cell Sci **114**(Pt 16): 2943-2951.

Grabsch, H., S. Takeno, W. J. Parsons, N. Pomjanski, A. Boecking, H. E. Gabbert and W. Mueller (2003). "Overexpression of the mitotic checkpoint genes BUB1, BUBR1, and BUB3 in gastric cancer--association with tumour cell proliferation." J Pathol **200**(1): 16-22.

Greene, A. K. and M. Puder (2003). "Partial hepatectomy in the mouse: technique and perioperative management." J Invest Surg **16**(2): 99-102.

Gregg, S. Q., V. Gutierrez, A. R. Robinson, T. Woodell, A. Nakao, M. A. Ross, G. K. Michalopoulos, L. Rigatti, C. E. Rothermel, I. Kamileri, G. A. Garinis, D. B. Stolz and L. J. Niedernhofer (2012). "A mouse model of accelerated liver aging caused by a defect in DNA repair." Hepatology **55**(2): 609-621.

Grisham, J. W. (1962). "A morphologic study of deoxyribonucleic acid synthesis and cell proliferation in regenerating rat liver; autoradiography with thymidine-H3." Cancer Res **22**: 842-849.

Guicciardi, M. E., H. Malhi, J. L. Mott and G. J. Gores (2013). "Apoptosis and necrosis in the liver." Compr Physiol **3**(2): 977-1010.

Guntani, A., T. Matsumoto, R. Kyuragi, K. Iwasa, T. Onohara, H. Itoh, Z. S. Katusic and Y. Maehara (2011). "Reduced proliferation of aged human vascular smooth muscle cells--role of oxygen-derived free radicals and BubR1 expression." J Surg Res **170**(1): 143-149.

Guntani, A., T. Matsumoto, R. Kyuragi, K. Iwasa, T. Onohara, H. Itoh, Z. S. Katusic and Y. Maehara (2011). "Reduced Proliferation of Aged Human Vascular Smooth Muscle Cells—Role of Oxygen-Derived Free Radicals and BubR1 Expression." J Surg Res **170**(1): 143-149.

Haga, S., N. Morita, K. Irani, M. Fujiyoshi, T. Ogino, T. Ozawa and M. Ozaki (2010). "p66(Shc) has a pivotal function in impaired liver regeneration in aged mice by a redox-dependent mechanism." Lab Invest **90**(12): 1718-1726.

Hanks, S., K. Coleman, S. Reid, A. Plaja, H. Firth, D. Fitzpatrick, A. Kidd, K. Mehes, R. Nash, N. Robin, N. Shannon, J. Tolmie, J. Swansbury, A. Irrthum, J. Douglas and N. Rahman (2004). "Constitutional aneuploidy and cancer predisposition caused by biallelic mutations in BUB1B." Nat Genet **36**(11): 1159-1161.

Hansemann, D. (1891). "Ueber pathologische Mitosen." (2): 356-370.

Hoyt, M. A., L. Totis and B. T. Roberts (1991). "S. cerevisiae genes required for cell cycle arrest in response to loss of microtubule function." Cell **66**(3): 507-517.

Hui, T. T., T. Mizuguchi, N. Sugiyama, I. Avital, J. Rozga and A. A. Demetriou (2002). "Immediate early genes and p21 regulation in liver of rats with acute hepatic failure." Am J Surg **183**(4): 457-463.

Incassati, A., D. Patel and D. J. McCance (2006). "Induction of tetraploidy through loss of p53 and upregulation of Plk1 by human papillomavirus type-16 E6." Oncogene **25**(17): 2444-2451.

Inoko, A., M. Matsuyama, H. Goto, Y. Ohmuro-Matsuyama, Y. Hayashi, M. Enomoto, M. Ibi, T. Urano, S. Yonemura, T. Kiyono, I. Izawa and M. Inagaki (2012). "Trichoplein and Aurora A block aberrant primary cilia assembly in proliferating cells." J Cell Biol **197**(3): 391-405.

Izumi, H., Y. Matsumoto, T. Ikeuchi, H. Saya, T. Kajii and S. Matsuura (2009). "BubR1 localizes to centrosomes and suppresses centrosome amplification via regulating Plk1 activity in interphase cells." Oncogene **28**: 2806.

Kakeji, Y., D. Korenaga, S. Tsujitani, H. Baba, H. Anai, Y. Maehara and K. Sugimachi (1993). "Gastric cancer with p53 overexpression has high potential for metastasising to lymph nodes." Br J Cancer **67**(3): 589-593.

Kamada, T., K. Sasaki, T. Tsuji, T. Todoroki, M. Takahashi and A. Kurose (1997). "Sample preparation from paraffin-embedded tissue specimens for laser scanning cytometric DNA analysis." Cytometry **27**(3): 290-294.

Kapanidou, M., S. Lee and V. M. Bolanos-Garcia (2015). "BubR1 kinase: protection against aneuploidy and premature aging." Trends Mol Med **21**(6): 364-372.

Karess, R. E., K. Wassmann and Z. Rahmani (2013). "New insights into the role of BubR1 in mitosis and beyond." Int Rev Cell Mol Biol **306**: 223-273.

Kops, G. J. P. L., D. R. Foltz and D. W. Cleveland (2004). "Lethality to human cancer cells through massive chromosome loss by inhibition of the mitotic checkpoint." Proc Natl Acad Sci U S A **101**(23): 8699-8704.

Kraniak, J. M., J. Abrams, J. E. Nowak and M. A. Tainsky (2006). "Antioxidant agents transiently inhibit aneuploidy progression in Li-Fraumeni cell strains." Mol Carcinog **45**(3): 141-156.

Kudela, M., R. Pilka, M. Lubusky, P. Hejtmanek, P. Dzubak and S. Brychtova (2012). "Prognostic importance of selected molecular immunohistochemical markers and DNA ploidy in endometrial cancer." Eur J Gynaecol Oncol **33**(2): 159-163.

Kupryjanczyk, J., A. D. Thor, R. Beauchamp, V. Merritt, S. M. Edgerton, D. A. Bell and D. W. Yandell (1993). "p53 gene mutations and protein accumulation in human ovarian cancer." Proc Natl Acad Sci U S A **90**(11): 4961-4965.

Kyuragi, R., T. Matsumoto, Y. Harada, S. Saito, M. Onimaru, Y. Nakatsu, T. Tsuzuki, M. Nomura, Y. Yonemitsu and Y. Maehara (2015). "BubR1 insufficiency inhibits neointimal hyperplasia through impaired vascular smooth muscle cell proliferation in mice." Arterioscler Thromb Vasc Biol **35**(2): 341-347.

Lampson, M. A. and T. M. Kapoor (2005). "The human mitotic checkpoint protein BubR1 regulates chromosome-spindle attachments." Nat Cell Biol **7**(1): 93-98.

Lechler, T. and E. Fuchs (2007). "Desmoplakin: an unexpected regulator of microtubule organization in the epidermis." J Cell Biol **176**(2): 147-154.

Lehmann, K., C. Tschuor, A. Rickenbacher, J. H. Jang, C. E. Oberkofler, O. Tschopp, S. M. Schultze, D. A. Raptis, A. Weber, R. Graf, B. Humar and P. A. Clavien (2012). "Liver failure after extended hepatectomy in mice is mediated by a p21-dependent barrier to liver regeneration." Gastroenterology **143**(6): 1609-1619.e1604.

Levine, A. J. (1997). "p53, the cellular gatekeeper for growth and division." Cell **88**(3): 323-331.

Li, A., M. Saito, J.-Z. Chuang, Y.-Y. Tseng, C. Dedesma, K. Tomizawa, T. Kaitsuka and C.-H. Sung (2011). "Ciliary transition zone activation of phosphorylated Tctex-1 controls ciliary resorption, S-phase entry and fate of neural progenitors." Nat Cell Biol **13**: 402.

Li, M., X. Fang, D. J. Baker, L. Guo, X. Gao, Z. Wei, S. Han, J. M. van Deursen and P. Zhang (2010). "The ATM-p53 pathway suppresses aneuploidy-induced tumorigenesis." Proc Natl Acad Sci U S A **107**(32): 14188-14193.

Li, R. and A. W. Murray (1991). "Feedback control of mitosis in budding yeast." Cell **66**(3): 519-531.

Liu, X., L. Pan, X. Wang, Q. Gong and Y. Z. Zhu (2012). "Leonurine protects against tumor necrosis factor-alpha-mediated inflammation in human umbilical vein endothelial cells." Atherosclerosis **222**(1): 34-42.

Matsumoto, T., D. J. Baker, L. V. d'Uscio, G. Mozammel, Z. S. Katusic and J. M. van Deursen (2007). "Aging-associated vascular phenotype in mutant mice with low levels of BubR1." Stroke **38**(3): 1050-1056.

Matsuo, T., S. Yamaguchi, S. Mitsui, A. Emi, F. Shimoda and H. Okamura (2003). "Control mechanism of the circadian clock for timing of cell division in vivo." Science **302**(5643): 255-259.

Matsuura, S., Y. Matsumoto, K. Morishima, H. Izumi, H. Matsumoto, E. Ito, K. Tsutsui, J. Kobayashi, H. Tauchi, Y. Kajiwara, S. Hama, K. Kurisu, H. Tahara, M. Oshimura, K. Komatsu, T. Ikeuchi and T. Kajii (2006). "Monoallelic BUB1B mutations and defective mitotic-spindle checkpoint in seven families with premature chromatid separation (PCS) syndrome." Am J Med Genet A **140**(4): 358-367.

Matsuura, S., Y. Matsumoto, K. Morishima, H. Izumi, H. Matsumoto, E. Ito, K. Tsutsui, J. Kobayashi, H. Tauchi, Y. Kajiwara, S. Hama, K. Kurisu, H. Tahara, M. Oshimura, K. Komatsu, T. Ikeuchi and T. Kajii (2006). "Monoallelic BUB1B mutations and defective mitotic-spindle checkpoint in seven families with premature chromatid separation (PCS) syndrome." Am J Med Genet A **140**(4): 358-367.

Meraldi, P., V. M. Draviam and P. K. Sorger (2004). " Timing and Checkpoints in the Regulation of Mitotic Progression." Dev Cell **7**(1): 45-60.

Meraldi, P., R. Honda and E. A. Nigg (2002). "Aurora-A overexpression reveals tetraploidization as a major route to centrosome amplification in p53-/- cells." EMBO J **21**(4): 483-492.

Michalopoulos, G. K. (2007). "Liver regeneration." J Cell Physiol **213**(2): 286-300.

Michalopoulos, G. K. and M. C. DeFrances (1997). "Liver regeneration." Science **276**(5309): 60-66.

Michel, L. S., V. Liberal, A. Chatterjee, R. Kirchwegger, B. Pasche, W. Gerald, M. Dobles, P. K. Sorger, V. V. Murty and R. Benezra (2001). "MAD2 haplo-insufficiency causes premature anaphase and chromosome instability in mammalian cells." Nature **409**(6818): 355-359.

Miyamoto, T., S. Porazinski, H. Wang, A. Borovina, B. Ciruna, A. Shimizu, T. Kajii, A. Kikuchi, M. Furutani-Seiki and S. Matsuura (2011). "Insufficiency of BUBR1, a mitotic spindle checkpoint regulator, causes impaired ciliogenesis in vertebrates." Hum Mol Genet **20**(10): 2058-2070.

Miyaoka, Y., K. Ebato, H. Kato, S. Arakawa, S. Shimizu and A. Miyajima (2012). "Hypertrophy and Unconventional Cell Division of Hepatocytes Underlie Liver Regeneration." Curr Biol **22**(13): 1166-1175.

Muroyama, A. and T. Lechler (2017). "Microtubule organization, dynamics and functions in differentiated cells." Development **144**(17): 3012-3021.

Musacchio, A. and E. D. Salmon (2007). "The spindle-assembly checkpoint in space and time." Nat Rev Mol Cell Biol **8**(5): 379-393.

Muschel, R. J., H. B. Zhang and W. G. McKenna (1993). "Differential effect of ionizing radiation on the expression of cyclin A and cyclin B in HeLa cells." Cancer Res **53**(5): 1128-1135.

Nigg, E. A. and J. W. Raff (2009). "Centrioles, Centrosomes, and Cilia in Health and Disease." Cell **139**(4): 663-678.

Ochiai, H., T. Miyamoto, A. Kanai, K. Hosoba, T. Sakuma, Y. Kudo, K. Asami, A. Ogawa, A. Watanabe, T. Kajii, T. Yamamoto and S. Matsuura (2014). "TALEN-mediated single-base-pair editing identification of an intergenic mutation upstream of BUB1B as causative of PCS (MVA) syndrome." Proc Natl Acad Sci U S A **111**(4): 1461-1466.

Oikawa, T., M. Okuda, Z. Ma, R. Goorha, H. Tsujimoto, H. Inokuma and K. Fukasawa (2005). "Transcriptional control of BubR1 by p53 and suppression of centrosome amplification by BubR1." Mol Cell Biol **25**(10): 4046-4061.

Perez de Castro, I., G. de Carcer and M. Malumbres (2007). "A census of mitotic cancer genes: new insights into tumor cell biology and cancer therapy." Carcinogenesis **28**(5): 899-912.

Pinto, M., J. Vieira, F. R. Ribeiro, M. J. Soares, R. Henrique, J. Oliveira, C. Jeronimo and M. R. Teixeira (2008). "Overexpression of the mitotic checkpoint genes BUB1 and BUBR1 is associated with genomic complexity in clear cell kidney carcinomas." Cell Oncol **30**(5): 389-395.

Rahmani, Z., M. E. Gagou, C. Lefebvre, D. Emre and R. E. Karess (2009). "Separating the spindle, checkpoint, and timer functions of BubR1." J Cell Biol **187**(5): 597-605.

Ralph, S. J., S. Rodriguez-Enriquez, J. Neuzil, E. Saavedra and R. Moreno-Sanchez (2010). "The causes of cancer revisited: "mitochondrial malignancy" and ROS-induced oncogenic transformation - why mitochondria are targets for cancer therapy." Mol Aspects Med **31**(2): 145-170.

Resnitzky, D., M. Gossen, H. Bujard and S. I. Reed (1994). "Acceleration of the G1/S phase transition by expression of cyclins D1 and E with an inducible system." Mol Cell Biol **14**(3): 1669-1679.

Roh, M., O. E. Franco, S. W. Hayward, R. van der Meer and S. A. Abdulkadir (2008). "A role for polyploidy in the tumorigenicity of Pim-1-expressing human prostate and mammary epithelial cells." PLoS One **3**(7): e2572.

Roh, M., R. van der Meer and S. A. Abdulkadir (2012). "Tumorigenic polyploid cells contain elevated ROS and ARE selectively targeted by antioxidant treatment." J Cell Physiol **227**(2): 801-812.

Rudolph, K. L., S. Chang, M. Millard, N. Schreiber-Agus and R. A. DePinho (2000). "Inhibition of experimental liver cirrhosis in mice by telomerase gene delivery." Science **287**(5456): 1253-1258.

Salogiannis, J. and S. L. Reck-Peterson (2017). "Hitchhiking: A Non-Canonical Mode of Microtubule-Based Transport." Trends Cell Biol **27**(2): 141-150.

Sanchez-Hidalgo, J. M., A. Naranjo, R. Ciria, I. Ranchal, P. Aguilar-Melero, G. Ferrin, A. Valverde, S. Rufian, P. Lopez-Cillero, J. Muntane and J. Briceno (2012). "Impact of age on liver regeneration response to injury after partial hepatectomy in a rat model." J Surg Res **175**(1): e1-9.

Sato, Y., S. Koyama, K. Tsukada and K. Hatakeyama (1997). "Acute portal hypertension reflecting shear stress as a trigger of liver regeneration following partial hepatectomy." Surg Today **27**(6): 518-526.

Satyanarayana, A., S. U. Wiemann, J. Buer, J. Lauber, K. E. Dittmar, T. Wustefeld, M. A. Blasco, M. P. Manns and K. L. Rudolph (2003). "Telomere shortening impairs organ regeneration by inhibiting cell cycle re-entry of a subpopulation of cells." EMBO J **22**(15): 4003-4013.

Schmucker, D. L. (2005). "Age-related changes in liver structure and function: Implications for disease ?" Exp Gerontol **40**(8-9): 650-659.

Schmucker, D. L. and H. Sanchez (2011). "Liver regeneration and aging: a current perspective." Curr Gerontol Geriatr Res **2011**: 526379.

Schvartzman, J. M., P. H. Duijf, R. Sotillo, C. Coker and R. Benezra (2011). "Mad2 is a critical mediator of the chromosome instability observed upon Rb and p53 pathway inhibition." Cancer Cell **19**(6): 701-714.

Sotillo, R., E. Hernando, E. Diaz-Rodriguez, J. Teruya-Feldstein, C. Cordon-Cardo, S. W. Lowe and R. Benezra (2007). "Mad2 overexpression promotes aneuploidy and tumorigenesis in mice." Cancer Cell **11**(1): 9-23.

Starzynska, T., M. Bromley, A. Ghosh and P. L. Stern (1992). "Prognostic significance of p53 overexpression in gastric and colorectal carcinoma." Br J Cancer **66**(3): 558-562.

Su, A. I., L. G. Guidotti, J. P. Pezacki, F. V. Chisari and P. G. Schultz (2002). "Gene expression during the priming phase of liver regeneration after partial hepatectomy in mice." Proc Natl Acad Sci U S A **99**(17): 11181-11186.

Suzuki, H., T. Nishizawa, H. Tsugawa, S. Mogami and T. Hibi (2012). "Roles of oxidative stress in stomach disorders." J Clin Biochem Nutr **50**(1): 35-39.

Tang, Z., R. Bharadwaj, B. Li and H. Yu (2001). "Mad2-Independent Inhibition of APCCdc20 by the Mitotic Checkpoint Protein BubR1." Dev Cell **1**(2): 227-237.

Taub, R. (2004). "Liver regeneration: from myth to mechanism." Nat Rev Mol Cell Biol **5**(10): 836-847.

Timchenko, N. A. (2009). "Aging and liver regeneration." Trends Endocrinol Metab **20**(4): 171-176.

Wang, Q., T. Liu, Y. Fang, S. Xie, X. Huang, R. Mahmood, G. Ramaswamy, K. M. Sakamoto, Z. Darzynkiewicz, M. Xu and W. Dai (2004). "BUBR1 deficiency results in abnormal megakaryopoiesis." Blood **103**(4): 1278-1285.

Wang, X., H. Kiyokawa, M. B. Dennewitz and R. H. Costa (2002). "The Forkhead Box m1b transcription factor is essential for hepatocyte DNA replication and mitosis during mouse liver regeneration." Proc Natl Acad Sci U S A **99**(26): 16881-16886.

Werner, S., A. Pimenta-Marques and M. Bettencourt-Dias (2017). "Maintaining centrosomes and cilia." J Cell Sci **130**(22): 3789-3800.

Yamamoto, Y., H. Matsuyama, Y. Chochi, M. Okuda, S. Kawauchi, R. Inoue, T. Furuya, A. Oga, K. Naito and K. Sasaki (2007). "Overexpression of BUBR1 is associated with chromosomal instability in bladder cancer." Cancer Genet Cytogenet **174**(1): 42-47.

Yu, H. (2002). "Regulation of APC-Cdc20 by the spindle checkpoint." Curr Opin Cell Biol **14**(6): 706-714.

Yuan, B., Y. Xu, J.-H. Woo, Y. Wang, Y. K. Bae, D.-S. Yoon, R. P. Wersto, E. Tully, K. Wilsbach and E. Gabrielson (2006). "Increased Expression of Mitotic Checkpoint Genes in Breast Cancer Cells with Chromosomal Instability." Clin Cancer Res **12**(2): 405-410.

Zhang, X., D. De Silva, B. Sun, J. Fisher, R. J. Bull, J. A. Cotruvo and B. S. Cummings (2010). "Cellular and molecular mechanisms of bromate-induced cytotoxicity in human and rat kidney cells." Toxicology **269**(1): 13-23.